NASA CONTRACTOR REPORT

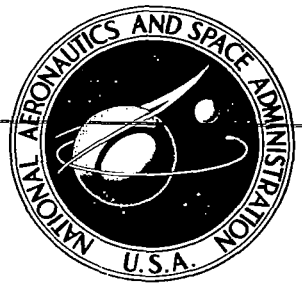

NASA CR-2

NASA CR-2883

DEVELOPMENT OF AN INTEGRATED CONFIGURATION MANAGEMENT/FLIGHT DIRECTOR SYSTEM FOR PILOTED STOL APPROACHES

Roger H. Hoh, Richard H. Klein, and Walter A. Johnson

Prepared by
SYSTEMS TECHNOLOGY, INC.
Mountain View, Calif. 90250
for Ames Research Center

NATIONAL AERONAUTICS AND SPACE ADMINISTRATION • WASHINGTON D. C. • AUGUST 1977

1. Report No.	2. Government Accession No.	3. Recipient's Catalog No.
NASA CR-2883		

4. Title and Subtitle	5. Report Date
"Development of an Integrated Configuration Management/Flight Director System for Piloted STOL Approaches"	August 1977
	6. Performing Organization Code
7. Author(s)	8. Performing Organization Report No.
Roger H. Hoh, Richard H. Klein and Walter A. Johnson	TR-1015-4
	10. Work Unit No.
9. Performing Organization Name and Address	11. Contract or Grant No.
Systems Technology, Inc. 13766 S. Hawthorne Blvd. Hawthorne, CA 90250	NAS 2-6441
	13. Type of Report and Period Covered
12. Sponsoring Agency Name and Address	Final Report
National Aeronautics and Space Administration Washington, DC 20546	14. Sponsoring Agency Code

15. Supplementary Notes

16. Abstract

A Systems analysis method for the development of an integrated configuration management/flight director system for IFR STOL approaches is presented. Curved descending decelerating approach trajectories are considered. Considerable emphasis is placed on satisfying the pilot centered requirements (acceptable workload) as well as the usual guidance and control requirements (acceptable performance). The Augmentor Wing Jet STOL Research Aircraft was utilized to allow illustration by example, and to validate the analysis procedures via manned simulation.

17. Key Words (Suggested by Author(s))	18. Distribution Statement
Curved Paths STOL Closed Loop Analysis Configuration Management Pilot Centered Requirements Guidance and Control Requirements Flight Director	UNCLASSIFIED - UNLIMITED STAR Category 08

19. Security Classif. (of this report)	20. Security Classif. (of this page)	21. No. of Pages	22. Price*
UNCLASSIFIED	UNCLASSIFIED	89	$4.00

*For sale by the National Technical Information Service, Springfield, Virginia 22161

TABLE OF CONTENTS

LIST OF FIGURES

LIST OF TABLES

SYMBOLS

a_x	Longitudinal acceleration as sensed by an accelerometer
a_y	Lateral acceleration as sensed by an accelerometer
a_z	Vertical acceleration as sensed by an accelerometer
d	Deviation of aircraft center of gravity from the glide slope; measured perpendicular to the glide slope
e	Napierian base
f	Function
F_s	Column (stick) force for longitudinal control
FD_c	Longitudinal column flight director command
FD_C	Output of bank angle limiter on lateral flight director
FD_w	Lateral flight director command
FD_T	Throttle flight director command
g	Acceleration due to gravity
G_x	Transfer function in feedback loop defined by a variable, x
h	Altitude
h_{select}	Altitude hold select (cockpit control)
K_x	Gain in feedback or feedforward loop defined by a variable, x
M	Blending circuit for transfer to backside operation (see Fig. 14)
N	Blending circuit for transfer from Altitude Hold to Glide Slope Tracking Mode (see Fig. 14)
OM, MM, IM	Outer, middle, and inner marker beacons associated with ILS approach system (see Fig. 37)
n_z	Normal load factor, g's
N_δ^x	Numerator of x/δ transfer function
p	Roll rate
q	Pitch rate

r	Yaw rate
R	Turn radius of circular course
s	Laplace operator
t	Time
T	Time constant
T	Time gain on longitudinal column flight director (see Fig. 14)
T_{WO} or T_W	Washout time constant
u	Change in velocity along x axis from U_O
U_O	Steady state velocity along x axis
v	Velocity along y axis
V or V_{TAS}	True airspeed
V_{IAS}	Indicated airspeed
V_{GS}	Groundspeed
V_{gs}	Groundspeed at glide slope capture
V_w	Wind velocity
V_{TW}	Tail wind component
V_{cal}	Calibrated airspeed
V_{select}	Commanded airspeed (cockpit control)
V_ϵ	Airspeed error (selected minus actual)
WP	Waypoint designator (see Fig. 37)
X, Y, Z	Inertial coordinates
X_{DIST}	Distance from aircraft c.g. to localizer antenna; measured along the path
y	Crosstrack deviation
y_c	Command lateral position
y_ϵ	Crosstrack error, $(y_c - y)$
$\dot{y}_A$	Actual crosstrack error rate, $[d/dt(y_c - y)]$

$\dot{y}_D$	Derived crosstrack error rate
Y_p	Transfer function representing human pilot
α	Angle of attack
β	Sideslip angle
γ or γ_a	Aerodynamic flight path angle
γ_I	Inertial flight path angle
δ_c	Longitudinal column deflection
δ_e	Elevator control surface deflection
δ_F	Flap deflection angle
δ_T or PLA	Cockpit throttle control angle (power lever angle)
δ_ν	Nozzle angle (0^o is full aft, 90^o is straight down)
δ_w	Lateral control wheel deflection angle
Δ	Characteristic determinant, denominator for transfer functions
ϵ_{loc}	Angle between aircraft c.g. and localizer centerline
ϵ_{GS}	Angle between aircraft c.g. and glide slope centerline
ζ	Damping ratio of second-order mode
θ	Pitch attitude
λ	Lateral flight path angle
σ	RMS value
τ	Human operator time delay
τ	Time constant in derived beam rate circuit for lateral flight directors
Φ_c	Feedforward bank angle command
Φ_{co}	Filtered bank angle command
φ	Aircraft bank angle
φ_{c_1}, φ_{c_2}	Defined in Fig.
φ_{wo}	Washed out bank angle
ψ	Heading angle

Ψ	Feedforward heading angle
ω_{sp}	Undamped natural frequency of short period mode
ω_{p}	Undamped natural frequency of phugoid mode
ω_{x}	Crossover frequency corresponding to feedback loop defined by x

Subscripts

aug	Refers to augmented airplane
GS	Groundspeed
c	Command
D	Desired
SAS	Stability augmentation system
o	Initial condition
R	Roll subsidence
$(\dot{})$	d/dt

Primed variables denote that their present value has resulted from a previously closed loop. The number of primes denotes more than one loop has been closed.

SECTION I

INTRODUCTION

The inherent complexity of the basic mission of STOL aircraft may give rise to an increase in requirements for improved flight control systems, displays, and control techniques. For example, the crew of a typical STOL transport may be faced with curved path, decelerating, high angle, precision approaches down to instrument minimums followed by a short-field landing on nearly every flight. Two fundamental concepts have evolved to achieve such performance with safety: first, a fully automatic system wherein the pilots simply act as monitors; and second, a system tailored around the pilot in such a way that the workload and task requirements for a manually controlled approach are reduced to an acceptable level. A third, and more expensive, choice is to do both, thereby allowing the pilots to take over and complete the STOL approach manually in the event of an automatic system failure. The work covered in the present report is oriented towards pilot-centered requirements and, accordingly, assumes the second concept where the pilot will be in the loop during the entire approach.

The major areas of concentration were centered about the design of improved flight director displays and configuration management techniques combined to minimize pilot workload.

Some of the fundamental concepts reported here represent an extension of earlier work. In particular, the basic formulation of the configuration management scheme is reported in Ref. 1 and the initial work on the longitudinal flight director is reported in Ref. 2.

The Augmentor Wing Jet STOL Research Aircraft presently being flown at NASA Ames Research Center served as the test bed for the conceptual developments and simulation reported herein. The analysis reflects this in that the airframe characteristics and high lift devices employed on that aircraft are utilized in the design development.

SECTION II

SYSTEM REQUIREMENTS

The fundamental requirements for the development of an integrated configuration management/flight director system have evolved over a period of years (e.g., Refs. 3-5). These requirements are summarized in this section with particular emphasis on application to powered-lift STOL airplanes which have descending, decelerating curved paths as a mission objective. The requirements consist of two fundamental subsets:

- Guidance and control requirements — fundamental and independent of whether the controller is an automatic or human pilot.
- Pilot-centered requirements — relate to the fact that the controller is a man.

A summary of the requirements central to design of these systems is given in Table 1. The satisfaction of these requirements from basic considerations leads to the selection, sensing, shaping, and relative weighting of appropriate feedbacks (and feedforwards) in a way which is best for manual control using the flight director/configuration management system.

A. GUIDANCE AND CONTROL REQUIREMENTS

These requirements are independent of the type of controller, manual or automatic. In general, they are such to establish the aircraft on a commanded path/speed profile, and to reduce any path errors to zero in a stable, well-damped manner. They lead to outer-loop feedbacks and command feedforwards which are required to accomplish the mission. Additional inner-loop feedbacks are needed to permit the first set of feedbacks to function.

Thus, for command following the system must accommodate:

- Curved and straight paths generated from the Microwave Landing System (MLS).
- Deceleration profiles on curved and straight paths during level flight and while tracking a steep glide slope.

TABLE 1

PILOT/VEHICLE SYSTEM REQUIREMENTS

Guidance and Control

- Command Following
- Disturbance Regulation
- Stability and Damping

Pilot-Centered

- Minimum Pilot Compensation
  - Feedbacks
  - Equalization
- Response Quality
- Frequency Separation of Controls
- Non-Interacting Controls
- Insensitivity to Pilot Response Variations
- Remnant Suppression

For disturbance regulation, the system must regulate against:

- Steady winds
- Random turbulence and gusts
- Horizontal wind shears

Stability and damping properties arise out of the inner loops and feedback of the rates of change (or derived rates) of outer-loop variables.

B. PILOT-CENTERED REQUIREMENTS

The presence of a human pilot in the control loop places additional requirements on the specification of the guidance and control laws. The following paragraphs treat briefly each of the pilot-centered requirements in Table 1.

1. Minimum Pilot Compensation

The desire to minimize pilot effort while retaining maximum system performance imposes requirements on the dynamic properties of the effective controlled element consisting of the vehicle plus flight director computer/display. As is well known, the human pilot adapts his characteristics to compensate for the dynamic deficiencies of the effective controlled element. As part of this adaptation, he may be forced to develop low-frequency lead(s) and/or to adjust his gain precisely. When low-frequency lead is required of the pilot, a cost in pilot dynamic capacity is incurred (Ref. 6) as reflected in increased effective time delay and a resulting deterioration in system performance. Pilot ratings also suffer somewhat from such decreased performance but mostly from the added "work" of low-frequency lead generation. Ratings may deteriorate further if the gains are in a non-optimum region (too sensitive or too sluggish).

As a result of these human pilot properties, an obvious design requirement is that the effective controlled element be constructed to:

- Require no low-frequency lead equalization.
- Permit pilot loop closure over a wide range of gains.

This can best be achieved when the effective controlled element (airplane plus SAS plus flight director) approximates a pure integration, K/s, over the frequency range of pilot/director/vehicle system crossover (see Ref. 7). This is accomplished by adjusting the weightings of the various feedbacks in the flight director computer so that the effective controlled element approximates this characteristic over a fairly broad frequency region.

Finally, the display/controlled-element dynamics should be approximately time invariant. The pilot can adjust to non-stationary situations, but it involves adaptation and learning which increases task difficulty and degrades performance. This implies that the beam error should be range compensated. The requirement for response quality must also be considered in the design of range compensation and is discussed in the following subsection.

2. Response Quality

Response quality refers to certain aspects of the display response and aircraft path response which directly affect the pilot's subjective opinion of the system. Those response qualities associated with the display are summarized below.

- Command bar consistency — Some correspondence must exist between the command signal and the vehicle or control motions in each of several frequency bands. At low frequency the command should be consistent with path deviation and aircraft heading. The mid-frequency response should be consistent with vehicle attitude motions and at high frequency with attitude rate or control displacement.

- Face validity — The command bar motions must be consistent with the status information without discontinuities or step commands that require large sudden control inputs (and/or result in attitude overshoots).

- Response compatibility — The command bar response should not require aggressive control activity nor should it appear "busy" to the pilot.

Response qualities associated with the resulting aircraft motions when the flight director is kept centered are given as follows.

- Modal interactions — The closed-loop system response should be rapid and well damped akin to that of a lower order system with minimum coupling between the modes of motion. This implies that the path mode and attitude modes should be well separated in frequency, i.e., piloted (using the flight director) or autopilot closure should not drive the system modes into near proximity to each other.

- Path mode consistency — The response of the system to an initial condition offset (due to an external disturbance, pilot inattention, etc.) should not result in "long tails," offsets, overshoots, or abrupt large attitude changes. Large attitude changes are indicative of a very "tight" system which tends to overdrive the bank or pitch angle. This is not consistent with normal IFR piloting technique and results in degraded pilot opinion and passenger comfort.

3. Frequency Separation of Controls

The frequency range of control for each longitudinal director should be separated. In this way one director is primary, e.g., for regulation of flight path, and the other director is for lower-frequency trim functions. This reduces the scanning workload between the two directors to an acceptable level. The importance of this requirement was reinforced during the piloted simulation phase of this program. That is, the pilots were very critical of director designs which involved reasonably tight manual control of speed and flight path. Allocating the speed control function to a speed SAS system met with very favorable pilot reaction.

4. Non-Interacting Controls

Each director should be essentially non-interacting, meaning that closure of one director loop will not produce an undesirable response on another director.

5. Insensitivity to Pilot Response

The pilot should be able to close the flight director loop over a wide range of crossover frequencies (gain) without a noticeable change in the path mode or flight director response. This implies a broad region of K/s over which the pilot can close the loop with an acceptable phase margin. Additionally, there should be no penalty for unattended operation such as would occur if beam integral were fed back to the flight director. In this case, if the pilot does not continually respond to the director commands, a small localizer deviation will be integrated to appear as a large director command. If the pilot then centers the bar, the aircraft is driven off the localizer to a point where the localizer error cancels the integrator output. The aircraft will then return to the beam with a time constant near that of the integral term (i.e., very slowly).

6. Remnant Suppression

Remnant is the pilot's output which is uncorrelated with his perceived error signal and may be of three kinds (Ref. 8) — residual, scanning, and

processing remnants. The most significant in the present context is scanning remnant which may be decreased by reducing the number of displays required to accomplish the desired task. This of course is the basic reason for having a flight director in the first place. The basic trade-off here is to maximize the amount of information on the flight director while maintaining a low level of complexity on the display. High-frequency control motions which are characteristic of pilot remnant should not show up when flying the flight director display. This is achieved in part by making the effective controlled element a K/s (e.g., high-frequency signals are filtered). Pure gain effective controlled elements (control position command on director) which do not attentuate high-frequency components tend to look very busy because of pilot remnant.

SECTION III

CONFIGURATION MANAGEMENT

The primary design goal of STOL transport aircraft is to achieve very low approach and landing speeds without significant sacrifice in cruise speed and payload. This implies some form of lift augmentation in the approach configuration. In many cases, this results in a redundant set of basic longitudinal controls, e.g., elevator, flaps, throttle, and other individual lift and drag control devices. Increased complexity of the piloting task arises from the number of control combinations which can be used to achieve a given trim state. In addition to having an extra control lever to manipulate, the pilot must also consider (and avoid) inadvertent excursions into "marginal regions" of the flight envelope. Unlike the CTOL aircraft situation where angle of attack and speed are directly related (1 g flight), the STOL pilot must consider a large variety of flight parameters to evaluate his current safety margins. The concept of the "configuration management" scheme discussed herein is to maximize the vehicle operating safety margins throughout the flight envelope from the "clean" configuration, through the conversion to STOL, and during straight and curved tracking of precision approach paths in the STOL mode. The objective is to provide the most operational flexibility in terms of climb and descent or acceleration and deceleration capability. A detailed description of the method is given in Ref. 1. The following paragraphs summarize the application of the "automatic" configuration management scheme to the Augmentor Wing Jet STOL Research Aircraft (Ref. 9 contains a description of this airplane) for a decelerating, descending, curved approach.

Primary consideration is given to minimizing pilot workload while maximizing the operating safety margins throughout the conversion to STOL and the final approach. The desired characteristics that accompany these objectives are summarized below:

- Controls which produce "separate" changes in airplane motion perpendicular and parallel to the velocity vector (this uncouples the controls).
- Good acceleration-deceleration and climb-descent capability (without coupling) at all speeds.

- Configurations that allow unsafe flight conditions should not be possible (due to configuration management scheme).
- Small changes in pitch attitude during transition for ride comfort and to maintain acceptable safety margins.
- Minimum number of required throttle changes.

A. FUNDAMENTAL CHARACTERISTICS

As discussed in detail in Ref. 1, the pilot workload is minimized by means of a flap-nozzle interconnect to keep the aircraft operating within the acceptable region of its trim envelope at any speed and descent combination.* The primary considerations in design of such an interconnect are:

1. The flap and the interconnected nozzle should be programmed as a function of speed.
2. Uncompensated flap deflections cause "ballooning." It is therefore desirable for the flap to lag rather than lead speed changes.
3. Flap actuation is slower than nozzle actuation; therefore, the flap should drive the nozzle for trim.
4. A continuous trim state is achieved by using the flap to also drive the elevator.
5. Speed regulation and command are best accomplished with the nozzle.

To summarize, a continuous trim state is best achieved by driving the flap with speed and in turn driving the nozzle and elevator with flap; speed perturbation from the trim state are handled by nozzle control.

A fundamental result is that the aircraft becomes neutrally stable in speed. Physically, this means that the aircraft will stay at its current

*The Augmentor Wing Aircraft utilizes a combination of blown flaps and thrust vector control for lift augmentation. The "nozzles" in this report refer to the hot thrust vector control. Reference to the nozzle is specialized to the Augmentor Wing but is generally applicable in principle to any fast acting independent lift/drag device.

airspeed until disturbed, in which case it will go to a new speed and automatically retrim for that flight condition. In terms of the characteristic modes of the aircraft, the phugoid roots are modified so that one pole is always near the origin. The resulting augmented aircraft is representative of a type one system (looks like an integrator) at low frequency. In fact, this was a primary objective of the design in that it serves as an ideal controlled element for speed command augmentation. The speed command system (which renders the configuration management scheme "automatic") is achieved via a unity feedback of airspeed which is compared with a selectable speed command signal and fed to the nozzle (δ_V, in the block diagram of Fig. 1). The functions f_1, f_2, f_3 in Fig. 1 define the previously mentioned flap, nozzle, and elevator interconnect required to achieve a continuous trim state. A gust filter $[1/(T_{L_u}s + 1)]$ was included to attenuate the effects of high-frequency gusts on the nozzle and flap servo actuators. A generic survey of the effect of the outer speed loop is given in Fig. 2. Note that the closed-loop pole at $1/T'_{u_1}$ is essentially cancelled by the zero at $1/T_{u_1}$, leaving only a dominant well-damped second-order mode. The speed SAS gain, K_{δ_V}, was selected to be constant for all flight conditions. The value was optimized during the FSAA simulation resulting in 10 degrees of nozzle per knot of airspeed error and a closed-loop speed mode of 0.69 rad/sec with a damping ratio of 0.72.

B. TRIM SCHEDULE DEVELOPMENT

The development of the trim schedules ($f_{1,2,3}$) involved a number of compromises between the pilot-centered and guidance and control requirements. In some cases, the desired performance was restricted by basic airplane limitations such as maximum deceleration capability, flap placards, and nozzle limits.

The primary restriction was the limited capability of the aircraft to decelerate on the glide path. The total acceleration along the velocity vector, $\dot{V}$, is given by:

$$\dot{V} = a_X - g\gamma$$

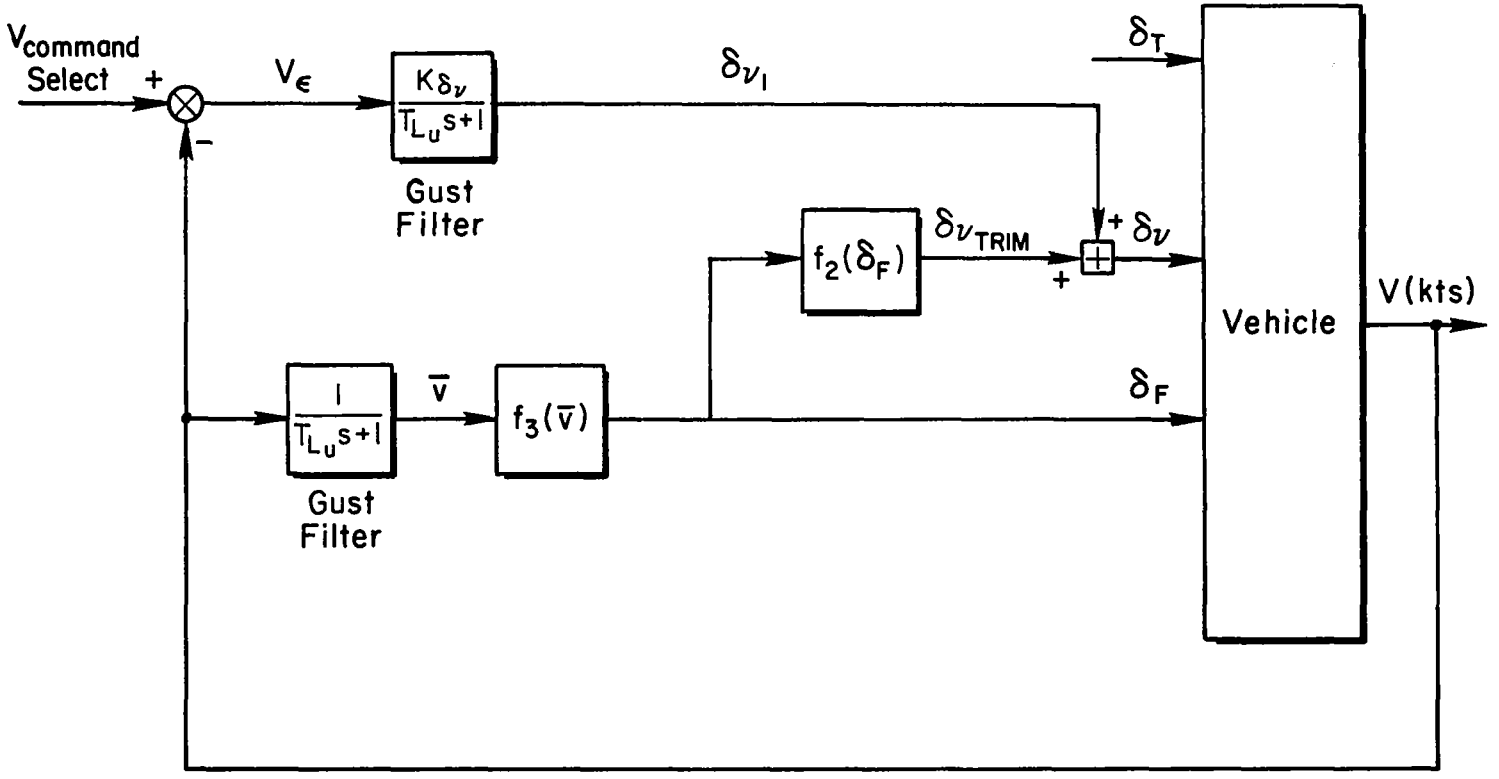

Note: f_1, f_2 and f_3 are functions derived from the trim curves in Figure 4 (for 140 > V > 60 kts)

Figure 1. Schematic Block Diagram of Automatic Speed Control System (Actuator Lags Are Not Shown)

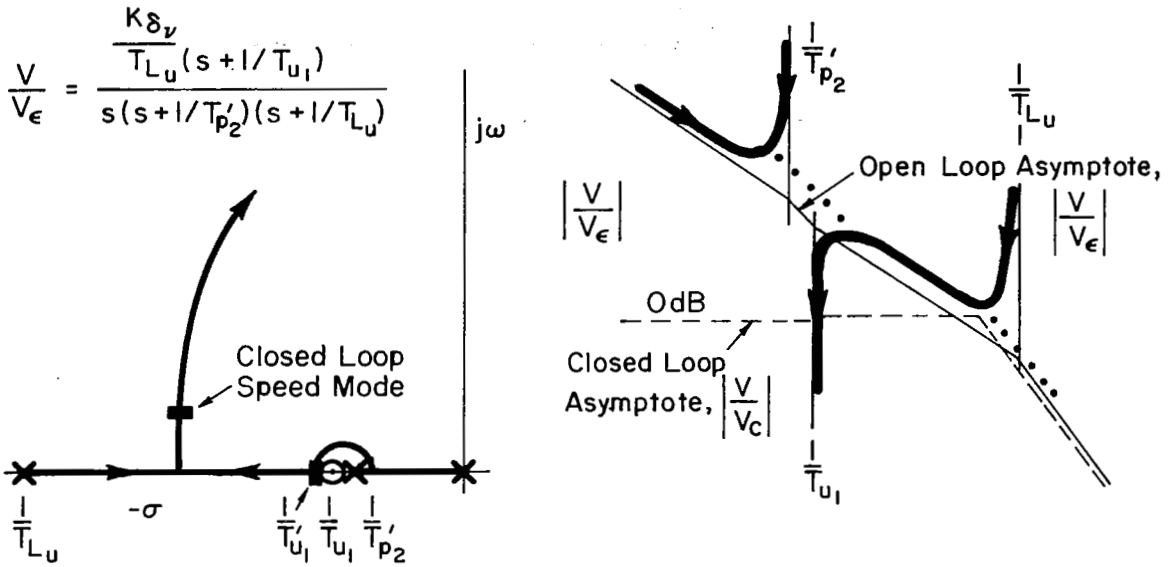

Figure 2. Generic Survey of Speed Command Loop

where a_x can be achieved with power, flap, and nozzle changes. Note that in level flight, all of the deceleration capability goes directly into speed changes, whereas in descending flight (negative γ) the maximum deceleration capability (negative $\dot{V}$) is decreased by $g\gamma$. This is shown graphically in the generic sketch in Fig. 3.

Figure 3 indicates that improved performance can be obtained if the pilot-centered requirements are ignored. That is, increased deceleration capability can be achieved via large changes in thrust and pitch attitude. The penalty is a significant increase in pilot workload and corresponding degradation in pilot opinion. The fundamental tradeoff centers about the ability to achieve an acceptable level of deceleration capability at glide slope intercept without incurring large variations in pitch attitude and thrust; and to maximize, as much as possible under such constraints, the allowable speed for glide slope intercept, V_{gs}. The final compromise does this for nominal winds (less than 25 kt). However, in the presence of a tailwind, γ is increased, and the $\dot{V}$ margin is reduced to the point where

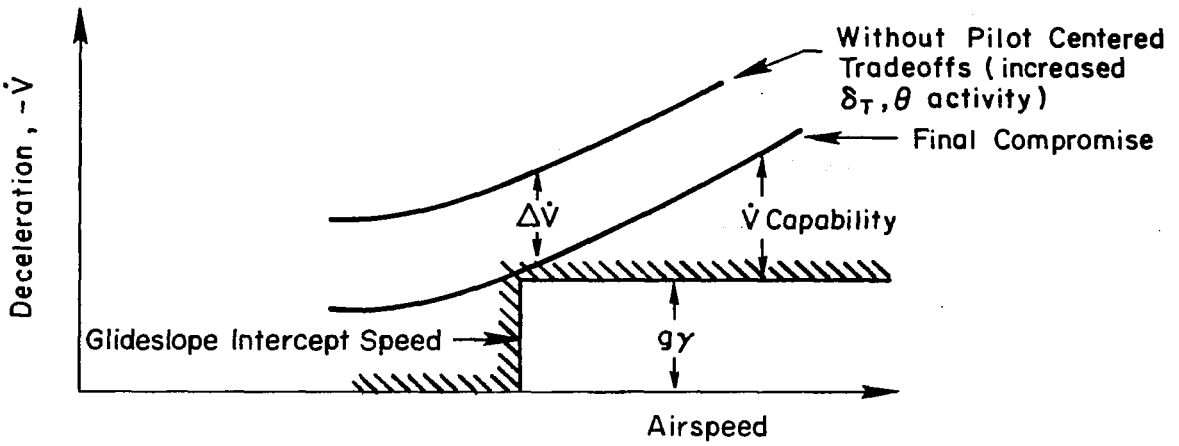

Figure 3. Effect of Glide Path Angle on Deceleration Capability

the aircraft will not decelerate below V_{gs} on the glide path. A practical solution is then to intercept the glide slope at a lower speed when this condition exists.

Attempts to maximize the deceleration characteristics via nozzle angle and thrust magnitude indicated that the resulting performance is fairly insensitive to the optimal combination. That is, going from high power settings and low nozzle angles to low power settings and high nozzle angles does not have a drastic effect on the maximum deceleration capability. Nevertheless, since the total deceleration capability is limited, some time was spent maximizing nozzle effectiveness.

In addition, the angle of attack was kept to a minimum value consistent with reasonable values of pitch attitude and power settings. This resulted in a trim angle of attack on the glide slope of 3 deg. The additional lift required for curved path tracking resulted in an α_{trim} of 5 deg. Abuses of the system which positioned the aircraft below the curved ILS course occasioned angles of attack as high as 8 deg, considered marginal but still in the acceptable range.

The nozzle, flap, and throttle trim curves which resulted from the above considerations are given in Fig. 4a and the resulting trim angle of attack

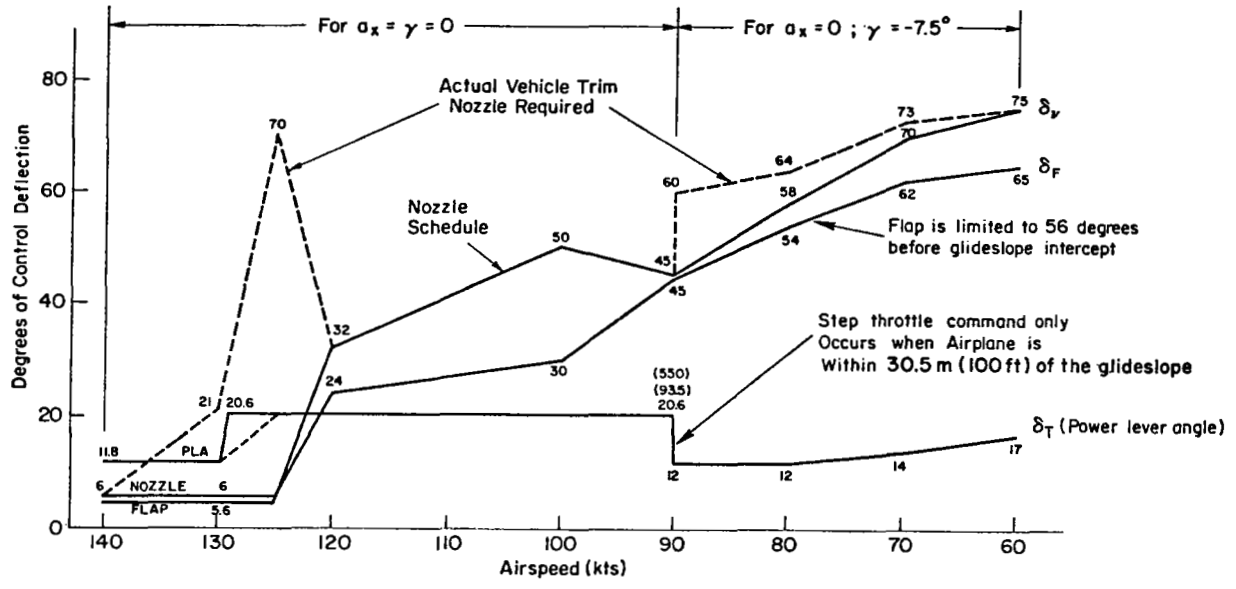

Figure 4a. Nozzle, Flap, and Throttle Trim Functions

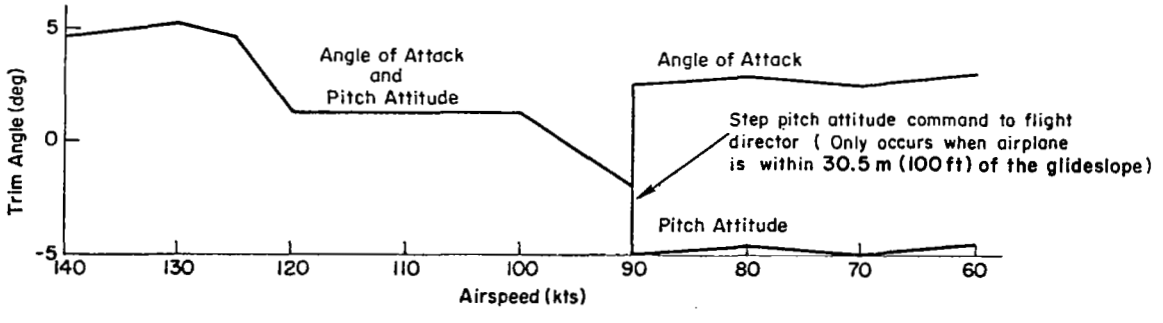

Figure 4b. Trim Angle of Attack and Pitch Attitude

and pitch attitude is shown in Fig. 4b. The dashed lines in Fig. 4a represent the ideal nozzle trim schedule required for perfect trim at all speeds. However, since the nozzles are driven by the flap (flap-to-nozzle crossfeed), no nozzle motion is possible when the flap rate is zero — hence the departure between the actual and ideal nozzle trim schedules. This results in some small speed standoffs (order of 5 kt) at speeds above 120 kt and has virtually no effect at speeds below 120 kt.

The final pilot-centered consideration involves frequency separation of controls (see Section II). Given a two-control task, the control effects should be decoupled and separated so that responses to the primary control occur at a much higher frequency than those to the secondary control. For speeds above 80 kt, altitude control is accomplished with pitch attitude, making elevator the primary control (the aircraft is inherently on the "front side" of the thrust-required curve). Accordingly, the throttle trim function was designed to be relatively inactive with only two discrete changes, one at 130 kt and the other at glide slope intercept. Below 80 kt, the control strategy is reversed and throttle becomes the primary regulatory control of altitude and/or glide slope. The trim pitch attitude is therefore a constant below 80 kt. The longitudinal flight director contains switching logic that changes the altitude/glide path feedback from the pitch bar to the throttle bug at 80 kt.

C. PILOTING TECHNIQUE

As noted above, the nozzle and flap controls are automatic and therefore not used by the pilot when the system is engaged. Speed changes are accomplished by slewing a speed command bug to the desired indicated airspeed and then keeping the pitch bar and throttle command bugs centered during the deceleration. If the aircraft is in the altitude hold mode, the pitch bar is the primary (most active) display until the aircraft decelerates below 80 kt at which time the throttle bug becomes primary and the pitch bar simply commands a reference attitude of about −2 deg. The same is true in the ILS mode except the pilot must not intercept the 7.5 deg glide slope at a speed above 90 kt to insure adequate deceleration capability on the glide slope for all wind conditions.

SECTION IV

LONGITUDINAL FLIGHT DIRECTOR

The longitudinal flight director system has been tailored to be compatible with the configuration management system in Section III and with certain flight path response characteristics of the example airplane (Augmentor Wing powered-lift STOL). The longitudinal director system provides both column and throttle commands throughout the entire approach from 140 kt level flight down to 60 kt on the glide slope. The various phases of the approach that the director must be designed for therefore include the following situations:

1. Altitude hold ($\gamma = 0$)
2. Conversion to STOL ($\gamma = 0$)
3. Glide slope capture ($\gamma = -7.5^{o}$)
4. Deceleration to final approach speed while maintaining glide slope ($\gamma = -7.5^{o}$)

A. AUGMENTED AIRCRAFT CHARACTERISTICS

In its present design, the aircraft augmentation consists of a speed control system utilizing an airspeed to hot thrust vector angle (nozzle) feedback for closed-loop control and a rate command attitude hold pitch SAS.

The steady-state flight path/airspeed characteristics for the Augmentor Wing are shown in Fig. 5 for a thrust vector angle of 90 deg and an approach flap setting of 65 deg. As is typical of powered-lift STOL's, the aircraft in Fig. 5 is trimmed well on the back side ($\partial\gamma/\partial V$ positive) at the approach flight condition.

The autospeed system in Fig. 1 tends to give the aircraft certain front-side characteristics, e.g., pitching up results in a decreased steady-state flight path angle. However, if the nozzle authority limits are exceeded or if the speed SAS fails, the aircraft characteristics return to those in

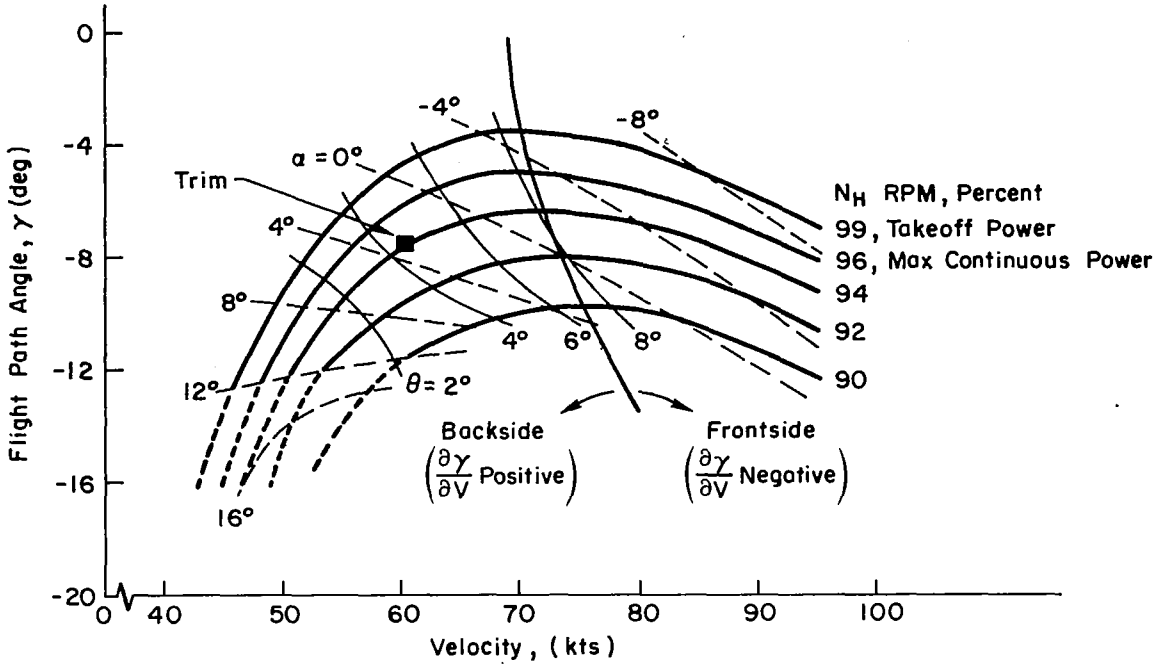

Figure 5. γ-V Characteristics of the Augmentor Wing Powered-Lift STOL

Fig. 5. Speed control systems on powered-lift STOL's are generally of limited authority because auxiliary control surfaces are required to produce the necessary longitudinal acceleration (thrust is nearly perpendicular to the flight path).

B. DESIGN ANALYSIS CONSIDERATIONS AND PROCEDURES

Two fundamental system concepts may be considered for flight path control. The more conventional of these is to mechanize the "backside" control technique into the flight director system, that is, to control glide slope errors via a power command bug on the flight director and airspeed errors via the pitch attitude command bar. An alternate concept is to feed back angle of attack to throttle to insure frontside operation (e.g., force θ and γ to track) and to control glide slope errors via the flight director pitch command bar. The control authority of this system is very large because the engine thrust is used as the primary feedback ($\alpha \rightarrow \delta_T$). This

latter concept is attractive because it involves a single command bar for longitudinal control and therefore inherently low workload. The former concept is simpler to mechanize and has the advantage of being a more direct approach (backside control technique for a backside airplane). Hence, the tradeoff at the outset is one of pilot workload vs. system complexity. It was decided to use the first concept (glide slope control with power command bug) because it represents a simpler mechanization and no change in pilot technique is required in the event of a SAS failure. The basic design goal in this concept is to minimize the complexity of the full-time automatic feedbacks (SAS) while keeping pilot workload at an acceptable level. Key design considerations for this concept are summarized below:

- Pilot workload is of primary importance, i.e., increased requirements for frequency separation of controls and non-interaction between the two longitudinal flight director commands.
- Flight path control is via the pitch command bar during frontside operation and the power command bug during backside operation. Blending between these modes of operation must be smooth and still supply adequate cues to alert the pilot to the change in commanded control technique.
- Saturation of the speed control system (thrust vector angle limiting) must not result in dangerous flight conditions.
- The flight director commands must be compatible with the configuration management program (shown in Fig. 4).

As discussed in Section III the configuration management scheme incorporates a full-time speed SAS which is mechanized by feeding airspeed to the hot thrust vector angle (nozzle). Hence, the requirement for airspeed control is effectively removed from the flight director and allocated as a SAS function. This has the very desirable effect of making the longitudinal flight director a single command display and resolves many of the pilot workload problems noted above.

Because of the relatively high gain required for effective speed control (10 deg of δ_V per kt of airspeed error, see Section III), thrust vector angle limiting is a relatively common event. Therefore, an airspeed feedback to the flight director pitch command bar is included to allow speed control

during periods of autospeed system saturation. This also serves to remove the requirement for redundancy in the airspeed SAS. The effect of pitch command bar motions during intermittent periods of autospeed system saturation was not found to be objectionable to the pilots.

The above discussion is primarily oriented toward the most demanding of the system requirements — glide slope tracking at STOL approach speeds well on the back side of the power-required curve. Other flight director functions occur at higher speeds where the aircraft is well on the front side ($\partial\gamma/\partial V$ negative). These are altitude hold, conversion to STOL from the cruise configuration, glide slope capture, and initial glide slope tracking. Flight path errors are fed back to the column director in these modes to take advantage of the inherent frontside characteristics. From Fig. 4a it can be seen that only two trim throttle positions are employed for speeds below 80 kt (12 percent power and 20.6 percent power). This was done intentionally when developing the configuration management program to insure that the pilot-centered requirement for separation of controls would be met. That is, the column director (pitch bar) is primary for flight path control, and the throttle director is secondary and serves only as a trim thrust command.

The transition from frontside control to backside control is based on the slope of the constant power lines in Fig. 5. For the example aircraft shown in Fig. 5 the inflection point is seen to vary from 70 to 75 kt. It was therefore decided to use 80 kt as the flight path control transition speed so that the column director is primary at speeds above 80 kt and the throttle director is primary at lower speeds.

A summary of considerations for selection of feedbacks to the longitudinal flight director is given in Table 2. Considerations for shaping and blending of the feedbacks in Table 2 are discussed in the following subsection.

C. PARAMETER ADJUSTMENT ANALYSIS

The analytical design procedure utilized to set the final system gains and feedback transfer functions was formulated to satisfy the requirements specified in Section II. These procedures are described below.

TABLE 2. CONSIDERATIONS FOR SELECTION OF LONGITUDINAL SYSTEM FEEDBACKS

FEEDBACKS	GUIDANCE AND CONTROL REQUIREMENTS		PILOT CENTERED REQUIREMENTS	
	PRIMARY REQUIREMENT	COMMENTS	PRIMARY REQUIREMENT	COMMENTS
Pitch Attitude, $\theta \rightarrow FD_C$	Short period attitude regulation	Must be washed out to avoid standoff between θ and d.	Command bar consistency	Mid-frequency flight director motions should look like pitch attitude
Pitch Attitude Rate, $\dot{\theta} \rightarrow FD_C$	Short period damping	Need to lag at high frequency to avoid a busy display	Minimum pilot compensation Remnant suppression	Provides K/s-like response at frequencies beyond the phugoid
Angle of Attack, $\alpha \rightarrow FD_T$	May be used as a linear protection circuit to avoid excessive angle of attack		Response quality	Will command proper action if angle of attack gets too large
Airspeed, $u \rightarrow FD_C$	Airspeed control	Backup for autospeed system	Frequency separation of controls	Will have to be low gain to avoid busy secondary control
Longitudinal Acceleration, $a_X \rightarrow FD_C$	High frequency windproofing	Complementary filter for airspeed feedback	Response quality	Allows filtering of high frequency airspeed information
Beam Rate, $\dot{d} \rightarrow FD_C$ or $\dot{d} \rightarrow FD_T$ if $(d\gamma/dV) \geq 0$	Vertical path damping	Beam noise is critical — may require complementary filter with a_Z	Minimum pilot compensation Path mode consistency Remnant suppression	Provides K/s-like effective controlled element
Beam Deviation, $d \rightarrow FD_C$ or $d \rightarrow FD_T$ if $(d\gamma/dV) \geq 0$	Vertical path following	Must be range compensated to avoid stability problems and still achieve required accuracy	Path mode consistency	Low frequency flight director should look like beam deviation
Beam Integration, $\int d\ dt \rightarrow FD_C$ or $\int d\ dt \rightarrow FD_T$ if $(d\gamma/dV) \geq 0$	Path angle trimming	Long time constant required for stability reduces regulation effectiveness.	Path mode consistency	Results in inconsistencies between command and beam errors after periods of unattended operation
Power Lever, $\delta_{RPM} \rightarrow FD_T$	None	None	Minimum pilot compensation Remnant suppression	Provides K/s response

1. Column Flight Director for Frontside Control (V_{IAS} > 80 kt)

From Table 2 the basic requirements for the column flight director (FD_c) are seen to involve feedback of pitch attitude and attitude rate for short-period regulation and beam deviation plus deviation rate for low- to mid-frequency path control. This is shown in block diagram form in Fig. 6.

A key objective of the parameter adjustment analysis is to insure that the shape of the frequency response of the effective controlled element (airplane plus flight director) to column inputs is K/s-like (−20 dB/dec slope) in the piloted crossover region. This allows the pilot's equalization requirements to be minimal as discussed in Section II. The transfer function which describes the flight director response to column inputs for the system shown in Fig. 6 is given as:

$$\frac{FD}{\delta_c} = K_{\dot{d}} \frac{N^{\dot{d}}_{\delta_c}\left(s^2 + \frac{1}{T_{L_d}}s + \frac{K_d}{K_{\dot{d}}}\frac{1}{T_{L_d}}\right)}{s\Delta\left(s + \frac{1}{T_{L_d}}\right)} + \frac{K_\theta\left(T_{L_{\dot\theta}} + \frac{K_{\dot\theta}}{K_\theta}\right)N^{\theta}_{\delta_c}s\left[s + \frac{1}{T_{L_{\dot\theta}} + (K_{\dot\theta}/K_\theta)}\right]}{\Delta\left(s + \frac{1}{T_{wo}}\right)\left(T_{L_{\dot\theta}}s + 1\right)} \quad (1)$$

where $N^{\theta}_{\delta_c}/\Delta$ and $N^{\dot{d}}_{\delta_c}/\Delta$ are the attitude and beam rate transfer functions with the rate command and speed SAS loop closed. The shape of the flight

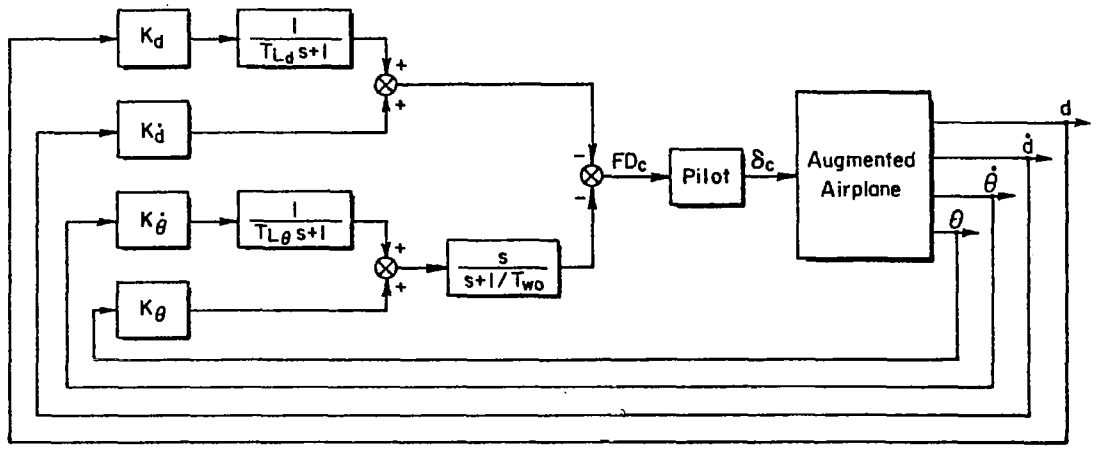

Figure 6. Basic Structure of Column Flight Director for Frontside Control

director to column frequency response depends on the zeros that result from summing the two terms in Eq. 1. This requires some fairly formidable algebra, making physical interpretation of feedback gain variations nearly impossible. A very good approximation to FD_c/δ_c can be obtained by ignoring the lags on the glide slope and pitch rate feedback (T_{L_d} and $T_{L_{\dot{\theta}}}$) and by noting that the augmented pitch attitude and beam rate to column transfer functions may be approximated as follows.

$$\frac{N^{\theta}_{\delta_c}}{\Delta} = \left(\frac{\theta}{\delta_c}\right)_{\substack{\theta \rightarrow \delta_e \\ u \rightarrow \delta_v}} \doteq \frac{K_{\delta_c}}{s} \tag{2}$$

$$\frac{N^{\dot{d}}_{\delta_c}}{\Delta} = \left(\frac{\dot{d}}{\delta_c}\right)_{\substack{\theta \rightarrow \delta_e \\ u \rightarrow \delta_v}} \doteq \frac{U_o K_{\delta_c}}{s(T''_{\theta_2} s + 1)} \tag{3}$$

The first of these expressions assumes that the rate command/attitude hold system is ideal (i.e., denominator poles are driven close to, and cancelled by, numerator zeros) in the region of piloted crossover. The second expression assumes that speed is being controlled perfectly. Under this condition the beam rate response to column is generally first-order with a path mode time constant given by the attitude numerator zero, $1/T_{\theta_2}$, as modified by the closures (double prime in Eq. 3 denotes that two loops — rate command and speed — have been closed). The complete transfer functions for θ/δ_c and $\dot{d}/\delta_c$ with the two loops closed are given in Appendix B. Cancellation of poles and zeros which are reasonably close and elimination of high-frequency (above 5 rad/sec) roots can be seen to result in the forms of Eqs. 2 and 3. Having made the above approximations, Eq. 1 may be put in root locus form to allow setting of the FD_c/δ_c zeros via graphical (root locus) factoring techniques:

$$1 + \frac{\frac{K_{\dot{d}}}{K_{\dot{\theta}}} \frac{U_o}{T''_{\theta_2}} \left(s + \frac{K_d}{K_{\dot{d}}}\right)\left(s + \frac{1}{T_{wo}}\right)}{s^2\left(s + \frac{K_\theta}{K_{\dot{\theta}}}\right)\left(s + \frac{1}{T''_{\theta_2}}\right)} = 0 \qquad (4)$$

A system survey which shows the effect of gain ($K_{\dot{d}}/K_{\dot{\theta}}$) variations is given in Fig. 7. The location of the resulting four closed-loop roots gives the zeros of FD_c/δ_c and hence the following generic expression.

$$\frac{FD_c}{\delta_c} = \frac{K_{\delta_c} K_\theta (s + 1/T_{FD_1})(s + 1/T_{FD_2})[s^2 + 2\zeta_{FD}\omega_{FD}s + \omega_{FD}^2]}{s^2(s + 1/T''_{\theta_2})(s + 1/T_{wo})} \qquad (5)$$

The approximate and exact FD_c/δ_c transfer functions for $K_{\dot{d}}/K_{\dot{\theta}} = 0.025$ are compared in Fig. 8. The Bode amplitudes are seen to agree very well, which is consistent with the analysis objective — to make FD_c/δ_c a K/s in the region of crossover. The lack of phase agreement at higher frequencies is due to actual system lags and is not important for our purposes.

Based on the root locus factoring in Fig. 7 and the generic form illustrated by Eq. 5 and Fig. 8, the selection criteria for system feedback gains and time constants may be summarized as follows.

- ω_{FD} should be set slightly below $1/T''_{\theta_2}$ to maximize the region of K/s. Values of $\omega_{FD} > 1/T''_{\theta_2}$ will result in a region of K/s^3 which is undesirable, both from a pilot-centered and a guidance and control standpoint. Since $1/T''_{\theta_2}$ is proportional to speed (see Ref. 10), ω_{FD} must also be proportional to speed to keep $\omega_{FD} \doteq (1/T''_{\theta_2})$. From Fig. 7 it can be seen that the $K_d/K_{\dot{d}}$ ratio in conjunction with $1/T_{wo}$ sets ω_{FD}. In the present flight director design, $K_{\dot{d}}$ is multiplied by V_o/V to allow ω_{FD} to track $1/T''_{\theta_2}$ as a function of speed.

- The flight director zero $1/T_{FD_1}$ must cancel $1/T''_{\theta_2}$ to preserve the K/s shape in the region of piloted crossover. From the Bode root locus in Fig. 7 this corresponds to keeping $K_{\dot{d}}/K_{\dot{\theta}}$ as low as practical with the constraint that ζ_{FD} must be some minimum value (on the order of 0.4).

$$1 + \frac{\frac{K_{\dot{d}}}{K_{\dot{\theta}}} + 95.83\,(.3)\,(.4)}{(0)^2\,(.63)\,(3.8)} = 0$$

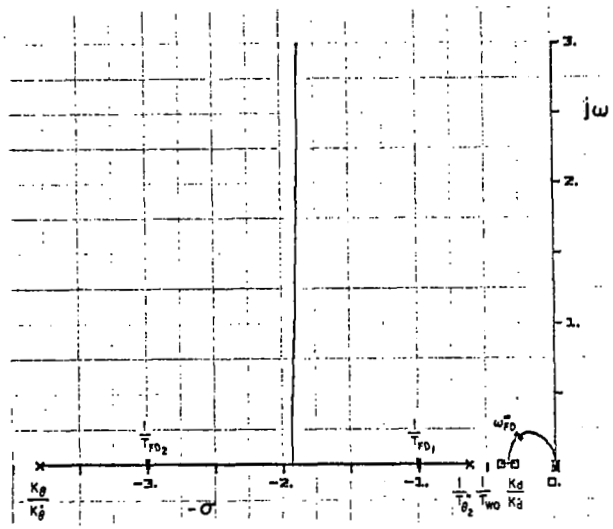

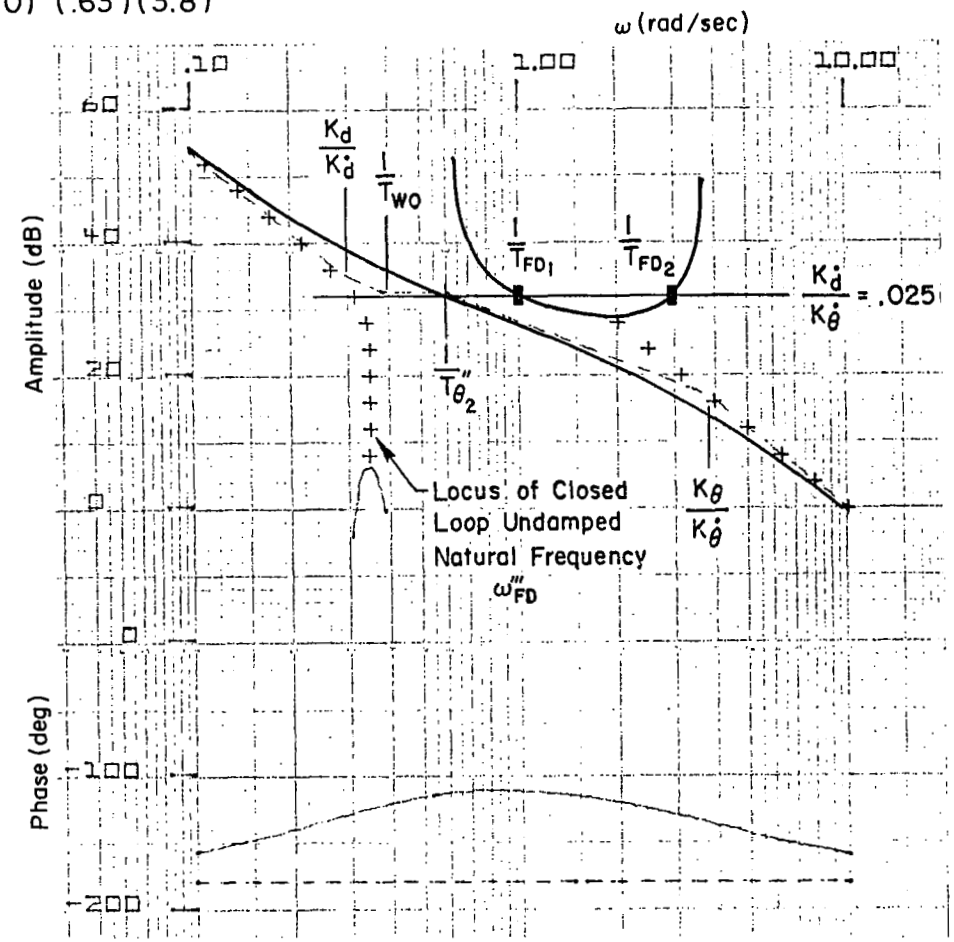

Figure 7. System Survey for Determination of Zeros of FD_c/δ_c

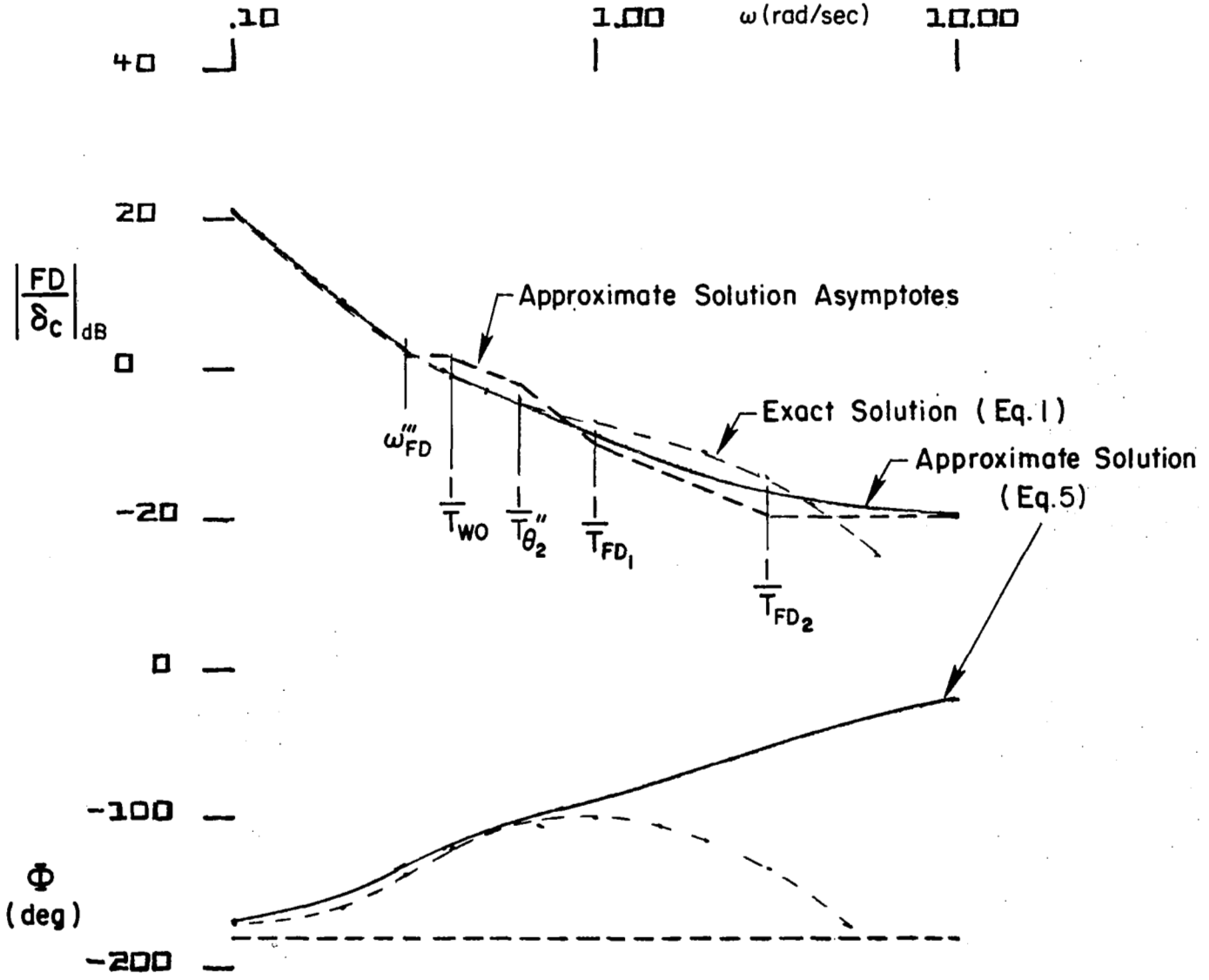

Figure 8. Exact and Approximate Solutions for Column Flight Director at 90 kt

- The approximate FD_c/δ_c transfer function becomes a pure gain at high frequencies above $1/T_{FD_2}$ (see Fig. 8), which is approximately equal to $K_\theta/K_{\dot{\theta}}$ (see Fig. 7). Therefore, $K_\theta/K_{\dot{\theta}}$ should be set to cancel system lags which occur at the upper end of the frequency range of interest, thereby tending to extend the K/s region. Setting $K_\theta/K_{\dot{\theta}}$ too low tends to flatten the FD_c/δ_c response (slope less than K/s) in the region of crossover, making the director look very busy due to amplification of pilot remnant (see Ref. 7).

The shape of FD_c/δ_c is determined, as above, by specifying ratios of the feedback gains ($K_d/K_{\dot{d}}$, $K_\theta/K_{\dot{\theta}}$, $K_{\dot{d}}/K_{\dot{\theta}}$). The magnitude of the flight director response in the frequency region near piloted crossover is set by K_θ to satisfy the command bar consistency requirement noted in Table 2. That is, the pitch command bar should look like attitude at attitude regulation frequencies. As an initial estimate, K_θ was set to .254 cm (0.1 in.) of FD_c per degree of pitch attitude [(K_θ = 14.48 cm)(5.7 in./rad)], which is reasonably close to the scaling on most attitude gyro displays. This was fine-tuned during the piloted simulation by varying the flight director display gain, K_{FD}, according to pilot commentary. The final setting was K_{FD} = 0.75, which turned out to be the actual scaling of the attitude gyro used [(0.275 deg/cm)(0.7 deg/in.)]. Once K_θ is specified then each of the individual feedback gains may be computed from the ratios obtained above.

It was found during the simulation that the pilots were quite sensitive to the value of $K_{\dot{\theta}}$. With $K_{\dot{\theta}}$ = 0 they complained that the director seemed too sluggish; conversely, excessive values of $K_{\dot{\theta}}$ elicited comments relating to a busy display. The effect of $K_{\dot{\theta}}$ on FD_c/δ_c is shown in Fig. 9. These results imply that the pilots like to see a K/s response out to about 3 rad/sec for the column flight director.

2. Column Flight Director During Backside Operation ($V_{IAS} \leq 79$ kt)

The column director plays a secondary role during operation in the backside mode and simply commands constant attitude. (The washout circuit in Fig. 6 is removed from the attitude feedback.) A low-gain airspeed feedback is also included in the column flight director. The purpose of this feedback is to provide a coarse speed control function during periods of speed SAS saturation and to regulate speed in the event of a speed SAS failure. Note

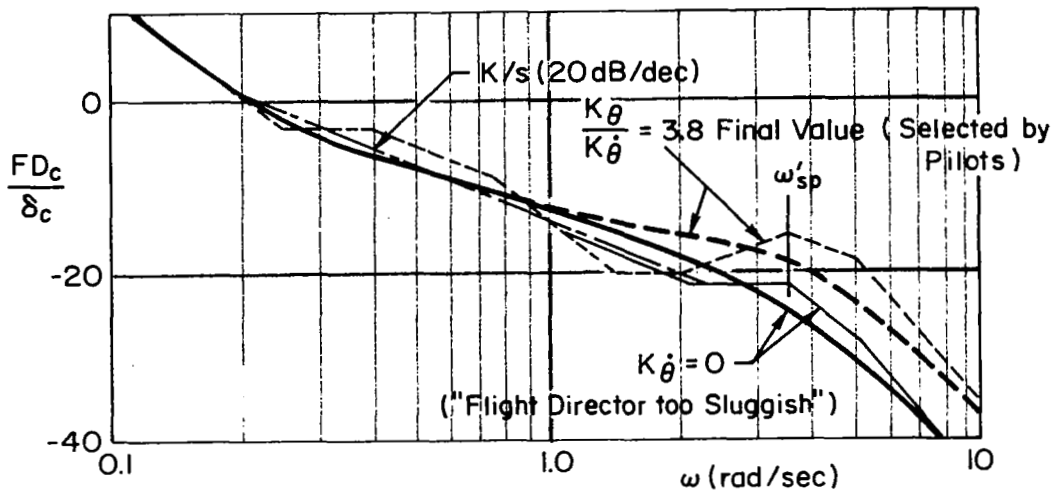

Figure 9. Effect of $K_{\dot\theta}$ on FD_c/δ_c

that this feedback effectively does not exist as long as the speed SAS is working to keep u = 0. A simplified block diagram illustrating the column flight director loop structure for backside operation is shown in Fig. 10.

It should be emphasized at this point that with the speed SAS operating, the column director will not be moving except to command an occasional change in trim pitch attitude per the configuration management schedule in Fig. 4. Consequently, the pilot will not be devoting any workload attention to the column director. This is a key aspect of the overall system design in that it provides for the satisfaction of the pilot-centered requirement for frequency separation of controls (see Section II). Attempts to use the flight director for speed control (speed SAS off and increased K_u) were found to be unacceptable to the pilots because of the extreme workload required to keep three active needles centered, and because the column director dynamics degrade with large values of K_u. The effect of airspeed feedback on the column director is illustrated in the following paragraph.

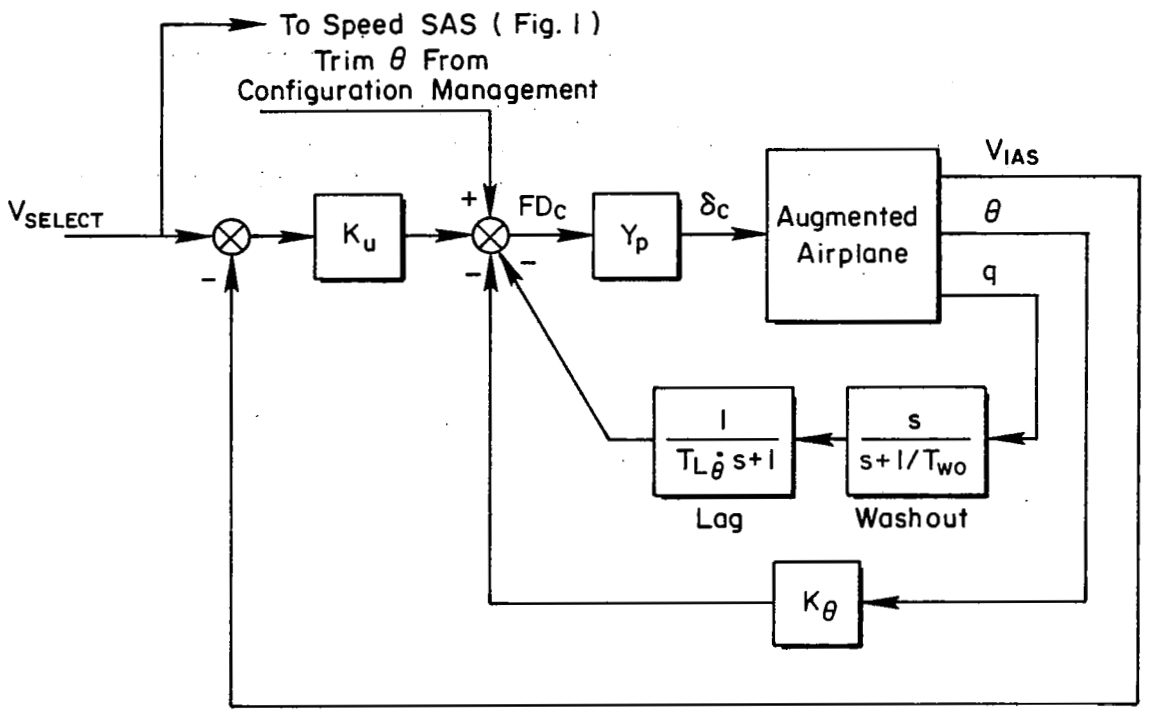

Figure 10. Column Flight Director for Backside Operation ($V_{IAS} \leq 79$ kt)

The effective controlled element of the column flight director with the speed feedback included is:

$$\frac{FD_c}{\delta_c} = \left[K_\theta + \frac{K_{\dot{\theta}} s^2}{(T_{L_{\dot{\theta}}} s + 1)(s + 1/T_{wo})} \right] \frac{\theta}{\delta_c} + K_u \frac{u}{\delta_c} \qquad (6)$$

The airspeed feedback gain, K_u, was set to achieve a steady state speed to attitude ratio of 3 [$K_u = 0.1/(\Delta U_{ss}/\Delta\theta_{ss}) = .1/3 = .033$ in./kt]. Using the same values of $T_{L_{\dot{\theta}}}$, T_{wo}, K_θ, and $K_{\dot{\theta}}$ as for frontside control results in the frequency characteristics in Fig. 11. Here it is shown that the response without airspeed feedback is K/s out to 3 rad/sec and that the effect of the airspeed feedback is a region of K/s^2 with an associated phase droop at low to mid frequency. This effect only appears intermittently (during speed SAS saturationθ and was not found to be objectionable by the pilots).

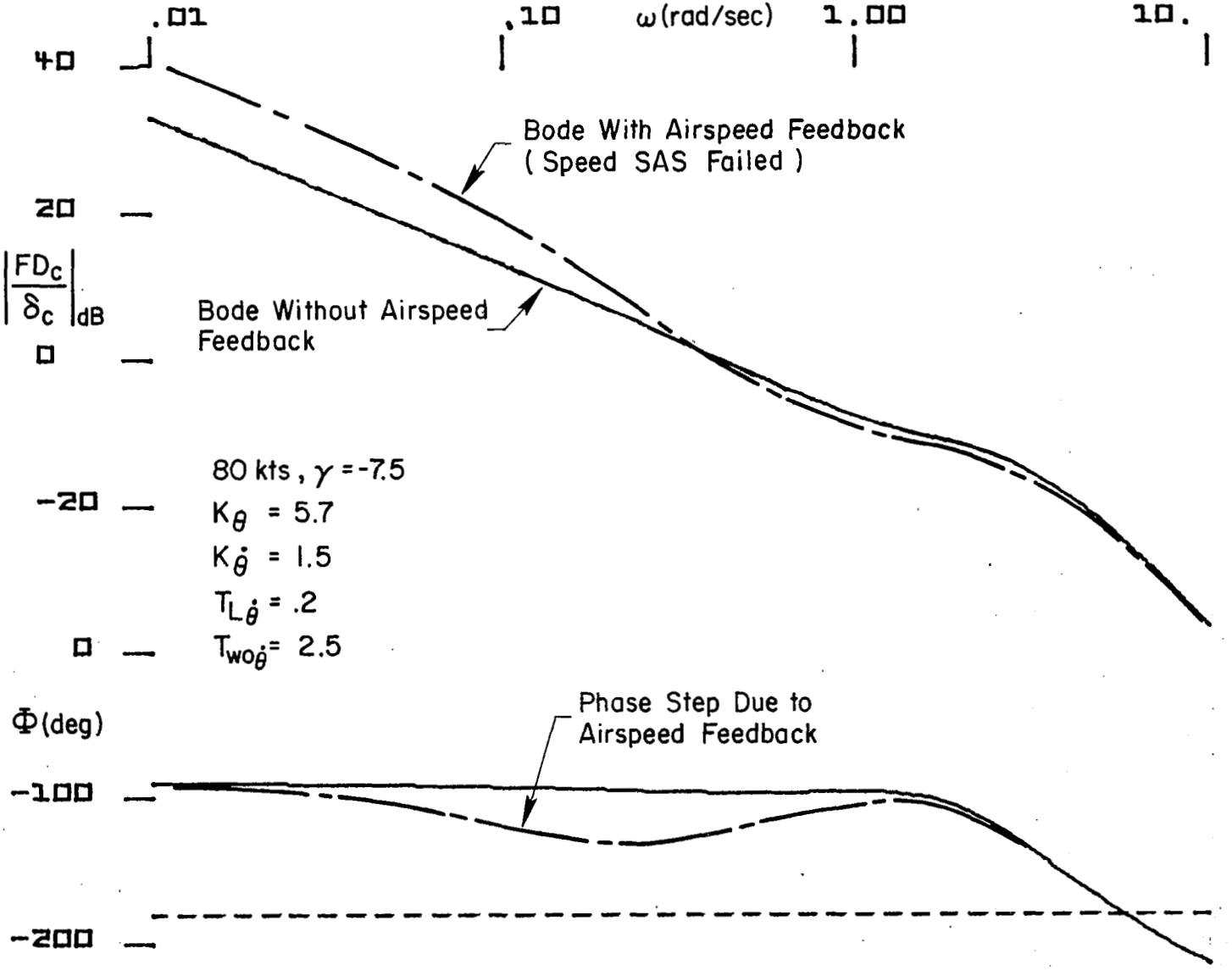

Figure 11. Comparison of Column Flight Director Response With and Without Airspeed Feedback — Backside Mode

3. Throttle Flight Director for Backside Control (V_{IAS} < 79 kt)

From Table 2 the basic requirements for the throttle flight director (FD_T) are seen to involve feedback of engine rpm for mid-frequency regulation and beam deviation plus deviation rate for path mode control. This is shown in block diagram form in Fig. 12. As with the column director, a key objective of the parameter adjustment analysis is to insure that the shape of the frequency response of the effective controlled element is K/s in the region of piloted crossover. The transfer function which describes the flight director response to throttle inputs for the system in Fig. 12 is given as:

$$\frac{FD_T}{\delta_T} = \frac{K_e K_{\delta_T} s}{(T_e s + 1)(s + 1/T_{wo})} + \frac{N^d_{\delta_T} K_e}{\Delta(T_e s + 1)} \left[s K_{\dot{d}} + \frac{K_d}{(T_{Ld} s + 1)} \right] \qquad (7)$$

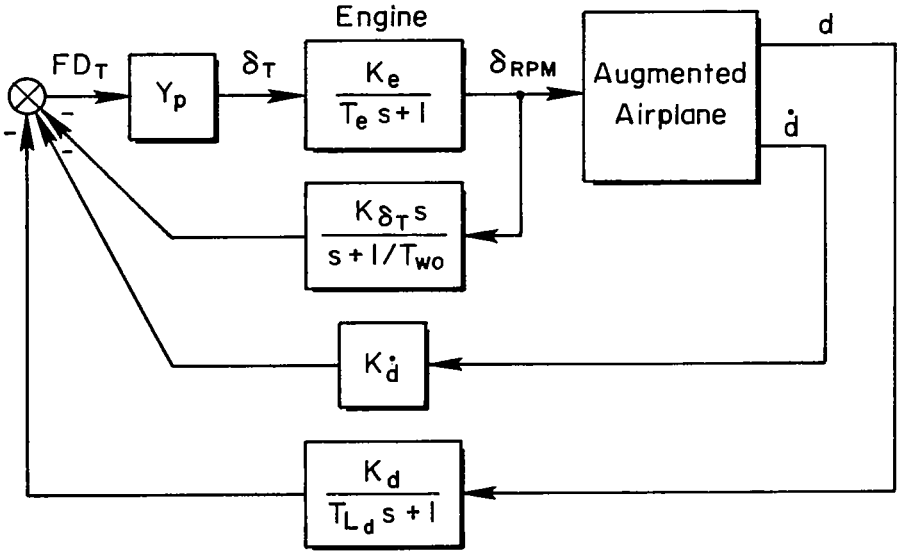

Figure 12. Basic Structure of Throttle Flight Director for Backside Control

where $N^{\dot{d}}_{\delta_T}/\Delta$ is the beam deviation to engine rpm response with the rate command/attitude hold pitch SAS and speed SAS loops closed. A very good approximation for this transfer function is given as:

$$\frac{N^{\dot{d}}_{\delta_T}}{\Delta} = \frac{\dot{d}}{\delta_{rpm}} \doteq \frac{-Z_{rpm}}{s + 1/T''_{\theta_2}} \tag{8}$$

The shape of the flight director to throttle frequency response depends on the zeros which result from summing the two terms in Eq. 7. Proceeding in the same manner as with the column director, Eq. 7 is put into root locus form for factoring as follows:

$$1 - \frac{(Z_{\delta_T} K_{\dot{d}}/K_{\delta_T}) \overbrace{[s^2 + (1/T_{L_d})s + (K_d/K_{\dot{d}})(1/T_{L_d})]}^{(s + 1/T_{d_1})(s + 1/T_{d_2})}(s + 1/T_{wo})}{s^2(s + 1/T''_{\theta_2})(s + 1/T_{L_d})} \tag{9}$$

The generic characteristics of the root locus factoring via the above expression is shown in Fig. 13. The literal expression for the factored FD_T/δ_T transfer function is obtained from Eq. 9 and Fig. 13 as:

$$\frac{FD_T}{\delta_T} = \frac{K_e K_{\delta_T}(s + 1/T'''_{\theta_2})(s + 1/T'''_{L_{\dot{d}}})[s^2 + 2\zeta'''_{FD}\omega'''_{FD}s + \omega'''^2_{FD}]}{s(T_e s + 1)(s + 1/T_{wo})(s + 1/T''_{\theta_2})(s + 1/T_{L_d})} \tag{10}$$

The primary objective in setting the zeros of FD_T/δ_T in Fig. 13 is to make Eq. 10 K/s over a broad region around piloted crossover. Requirements on the feedback gains and time constants to accomplish this objective may be inferred from Fig. 13 and Eq. 10 as follows.

- Set $1/T_{wo}$ and $1/T_{d_1}$ approximately equal to $1/T''_{\theta_2}$ so that ω'''_{FD} nearly cancels $1/T_{wo}$ and $1/T''_{\theta_2}$ in Eq. 10.
- Make $K_{\dot{d}}/K_{\delta_T}$ large enough to drive ω'''_{FD} into the vicinity of the pair of zeros, $1/T_{wo}$ and $1/T_{d_1}$.

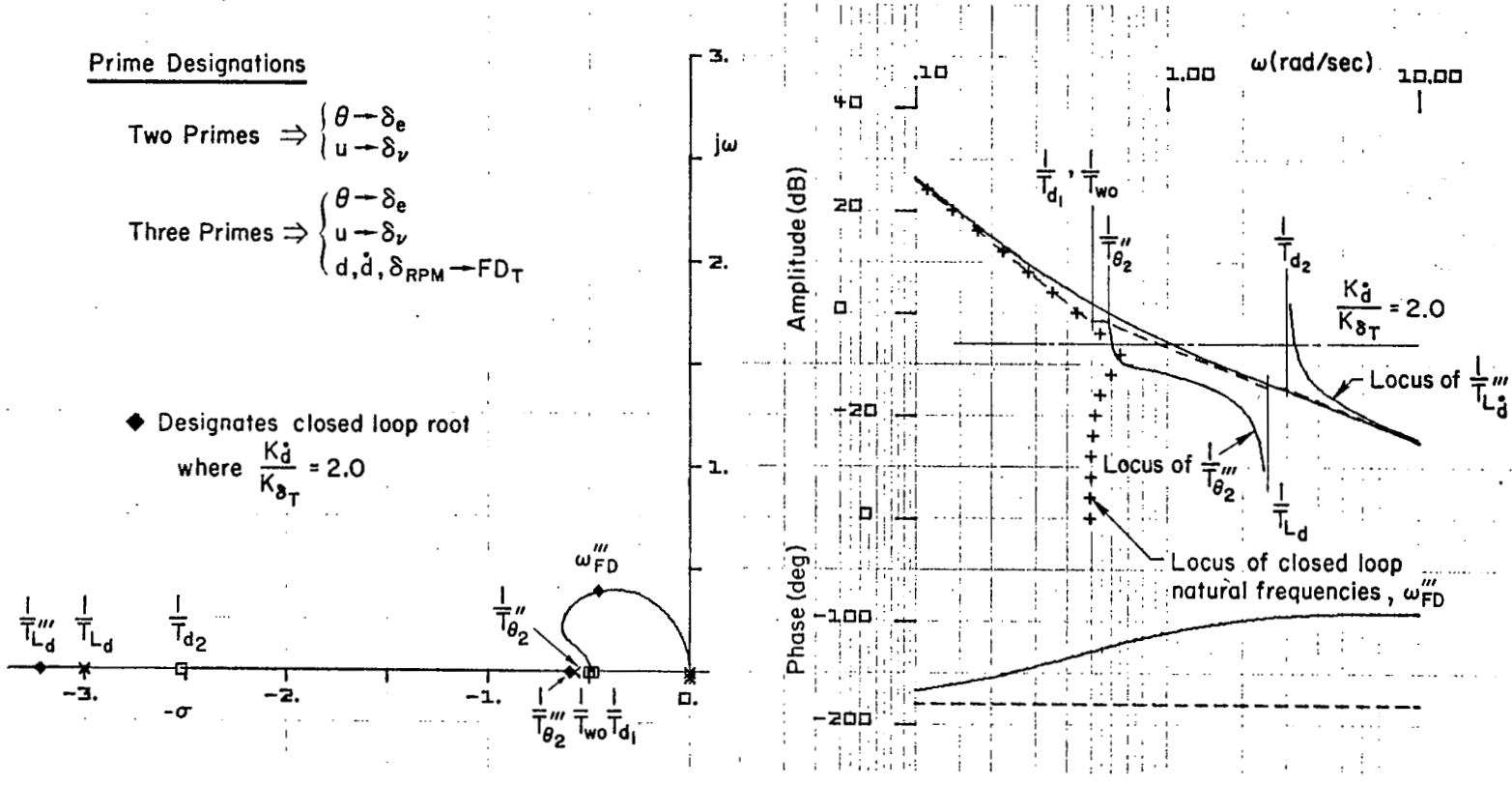

Figure 13. Generic Characteristics of FD_T/δ_T Zero Variation with $K_{\dot{d}}/K_{\delta T}$

- An upper bound on $\dot{K}_d/K_{\delta_T}$ is set by the requirement to keep $1/T_{\theta_2}''$ in the vicinity of $1/T_e$. Values of $1/T_{\theta_2}''' > 1/T_e$ result in a K/s^2 Bode asymptote between $1/T_e$ and $1/T_{\theta_2}'''$ in the FD_T/δ_T response.

- Factor $[s^2 + (1/T_{L_d})s + (K_d/\dot{K}_d)(1/T_{L_d})]$ so that the $1/T_{d_1}$ root is near $1/T_{wo}$ (as previously discussed) and the $1/T_{d_2}$ root is above the region of crossover (FD_T/δ_T is K/s^2 above $1/T_{d_2}$ when $1/T_{d_2}$ is low). This basically sets the lower limit on $1/T_{L_d}$.

The result obtained by setting the gains and time constants for the example airplane based on the above requirements is shown in Fig. 14.

The actual development of the throttle flight director evolved in several stages, resulting in the design philosophy discussed above. However, it was initially thought that the overriding requirement would be to keep the effective controlled element essentially constant across the transition from frontside control to backside control. Since the throttle director served as a trim thrust command during frontside operation (and therefore a pure gain effective controlled element) it was felt that the effective controlled element should be a pure gain for backside control. The initial design (Ref. 11) reflects this approach. Piloted evaluations were actually reasonably good during the Ref. 11 study, indicating that a pure gain throttle director is not unacceptable. Based on the Ref. 11 results, this concept was utilized in a subsequent generic STOL handling study (Ref. 12) which involved extensive evaluation by four pilots on several different powered-lift STOL configurations. Pilot commentary during this study tended to support some offhanded comments during the Ref. 11 evaluations, e.g., that the pure gain throttle director left something to be desired. Specifically, the pilots noticed that the director could be centered immediately but that it would invariably "drift off," requiring constant power corrections. A throttle flight director having an effective controlled element with a K/s shape was designed and implemented with considerable improvement noted by the pilots. The K/s shape in this director was achieved by eliminating the engine rpm feedback. This resulted in a K/s shape, but only out to the engine lag frequency, resulting in a bandwidth limited display. This deficiency was noted in the pilot commentary which indicated that the director seemed a little sluggish. The present throttle director design (Fig. 14) utilizes engine

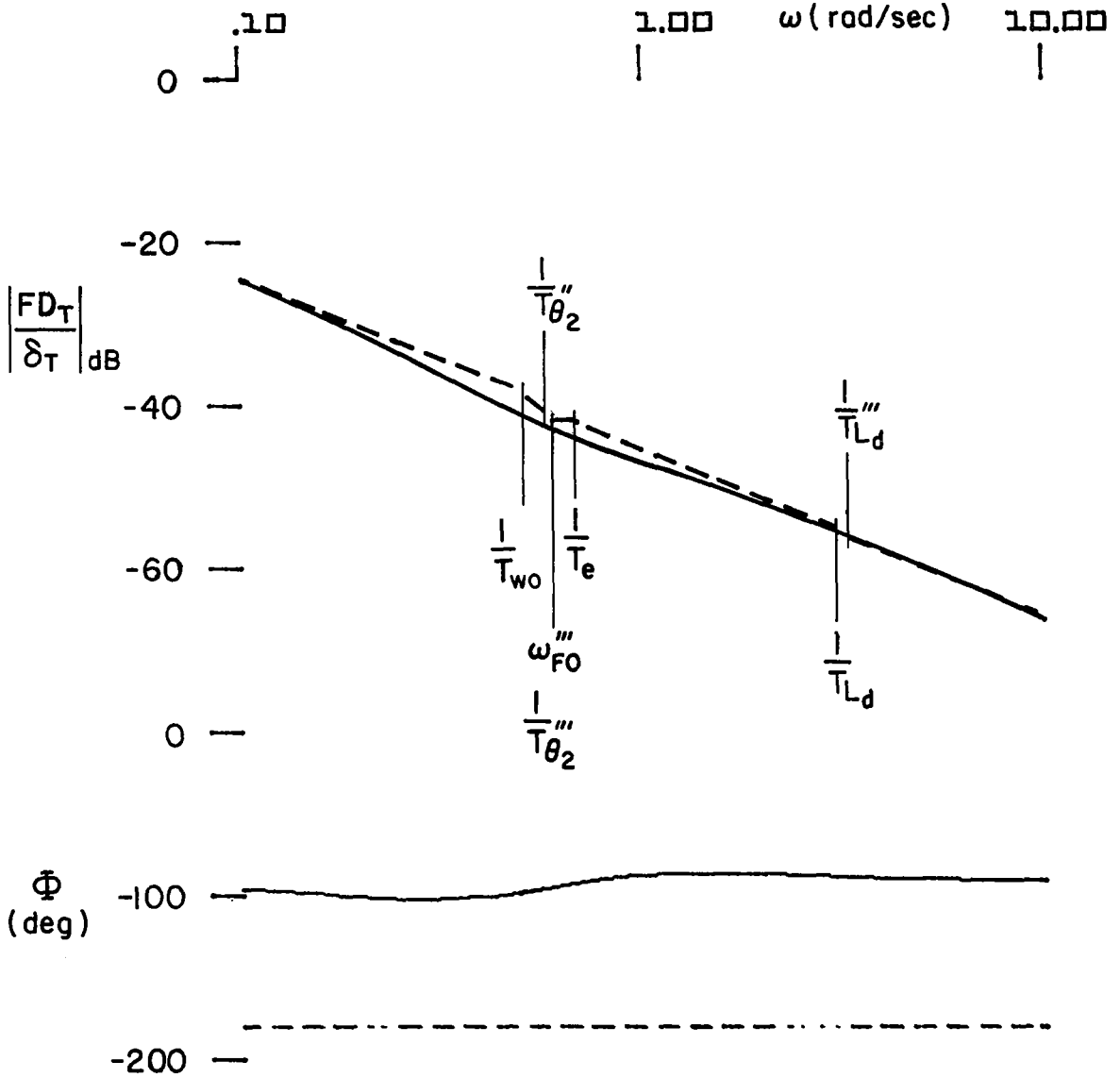

K_d = .095 cm/m (.0114 in./ft)

$K_{\dot{d}}$ = .242 cm/m/sec (.029 in./ft/sec)

K_{δ_T} = .038 cm/% rpm (.015 in./% rpm)

K_e = .52% rpm/deg δ_T

T_{wo} = 2.0 sec

T_e = 1.5 sec

T_{L_d} = .33 sec

Figure 14. Effective Controlled Element for Throttle Flight Director at 60 kt on a -7.5 deg Glide Slope

rpm feedback to extend the region of K/s past the engine lag frequency. Both simulator and flight evaluations of this director have resulted in excellent pilot acceptance.

D. FLIGHT DIRECTOR LOGIC FUNCTIONS

1. Column Flight Director

The block diagram and backside/frontside switching logic for the final version of the column flight director are given in Fig. 15.

The M functions in Fig. 15 serve to transfer the column director from a flight path angle control with pitch attitude technique at $V_{IAS} > 80$ kt to a "constant attitude mode" at $V_{IAS} < 79$ kt. In the present mechanization, the M function is essentially a switch since the blending occurs over only one knot. This is a result of simulation which showed that blending over a wider speed range to avoid flight director discontinuities at the switch point was not necessary. The "constant attitude mode" contains some airspeed error feedback to help the automatic speed control system during backside operation. A ±10 kt limiter is used on this feedback to keep attitude excursions at or below ±3 deg from trim. The V_{select} input used to form the speed error is lagged to avoid a pitchup command when a lower speed is selected during backside operation.

The N function, in conjunction with the timer, T, and the latching switch (ISW) fades out the altitude hold signal as a function of beam deviation and blends in the glide slope tracking circuits as a linear function of time. T has a value of unity for all times greater than 15 sec past glide slope capture initiate [d < 30 m (100) ft] and is reset to zero when any mode except glide slope track is engaged.

The altitude hold mode is designed to maintain the altitude existing at mode engagement, that is, the circuit in Fig. 15 outputs zero altitude error until altitude hold is engaged.

An attitude limiter (Fig. 15, Insert 1) is included in the mechanization to protect against large attitude excursions about trim which might occur if

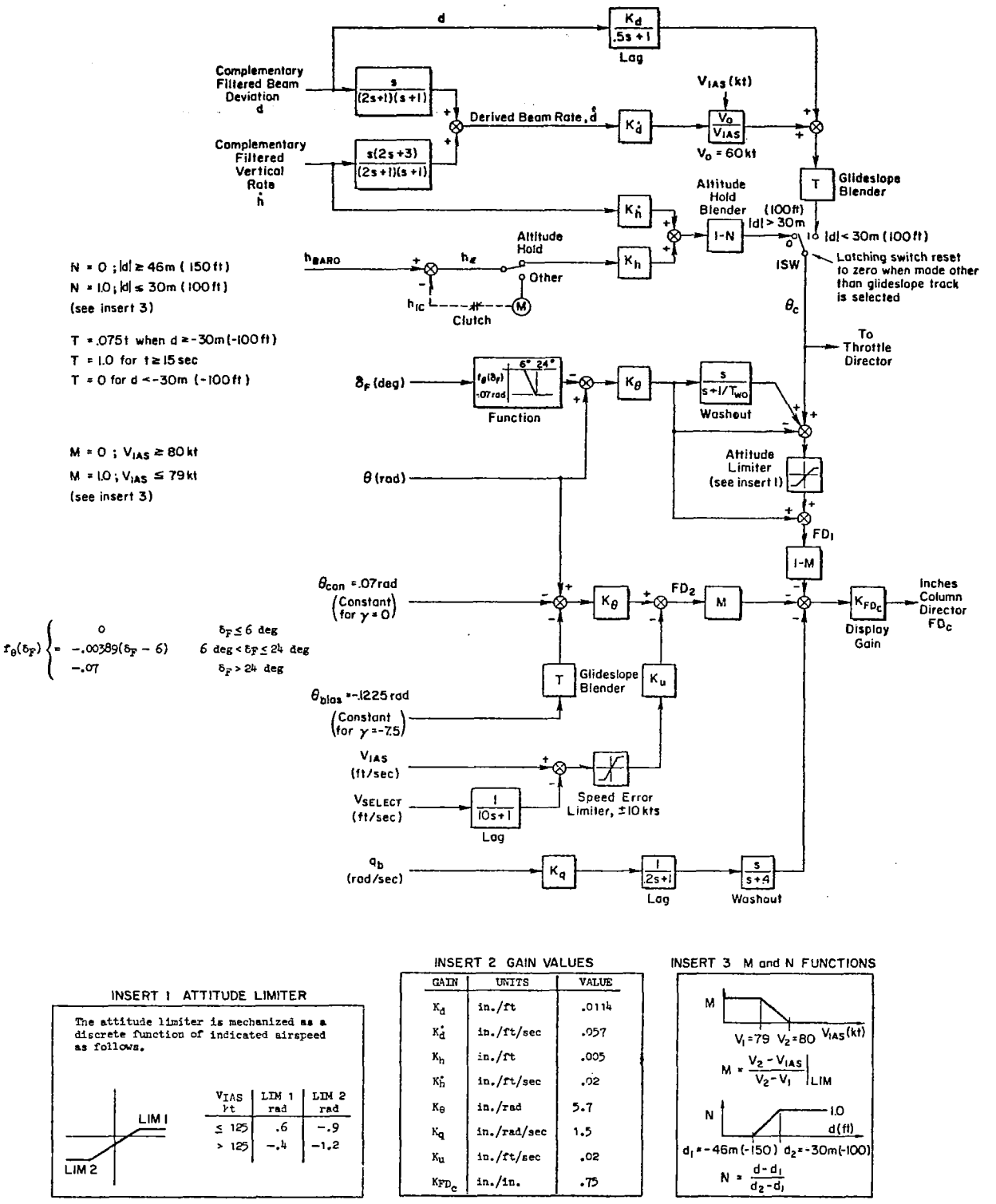

INSERT 1 ATTITUDE LIMITER

The attitude limiter is mechanized as a discrete function of indicated airspeed as follows.

V_{IAS} kt	LIM 1 rad	LIM 2 rad
≤ 125	.6	-.9
> 125	-.4	-1.2

INSERT 2 GAIN VALUES

GAIN	UNITS	VALUE
K_d	in./ft	.0114
$K_{\dot{d}}$	in./ft/sec	.057
K_h	in./ft	.005
$K_{\dot{h}}$	in./ft/sec	.02
K_θ	in./rad	5.7
K_q	in./rad/sec	1.5
K_u	in./ft/sec	.02
K_{FD_c}	in./in.	.75

INSERT 3 M and N FUNCTIONS

Figure 15. Complete Column Flight Director

large displacements from the commanded path occur. The limiter values are changed at 125 kt to account for the moderate change in trim pitch attitude which occurs at that speed (see Fig. 4b). Once the speed goes below 79 kt the limiter is removed from the flight director via the (1 − M) circuit.

The flap function $f_\theta(\delta_F)$ is an open-loop 4 deg pitch down command consistent with the change in trim pitch attitude (from 6 deg to 2 deg) as the aircraft is slowed from 125 kt to 120 kt (see Fig. 4b). Similarly, the θ_{con} and θ_{bias} inputs sum to give the appropriate trim pitch attitudes for constant altitude and glide path tracking at speeds below 80 kt (M = 1).

2. Throttle Flight Director

The block diagram and backside/frontside switching logic for the throttle flight director are given in Fig. 16. The M functions in the throttle director are configured to command trim thrust at speeds above 80 kt and altitude/glide path control below 79 kt (backside).

Thrust is measured and fed back via engine rpm. It should be noted that all of the initial system design and simulation was accomplished using power lever angle position feedback. However, the final simulation included recent data on throttle hysteresis effects which proved to be bothersome on the flight director display.

The maximum rpm limiter is included to eliminate the possibility of commanding more than maximum continuous rated thrust (96 percent rpm on the example aircraft) while using the backside control technique (M = 1).

An angle-of-attack protection feedback is included in the thrust director to minimize the possibility of getting into a dangerously high angle-of-attack situation. This feedback is summed downstream of the rpm limiter and therefore may command 100 percent power if necessary.

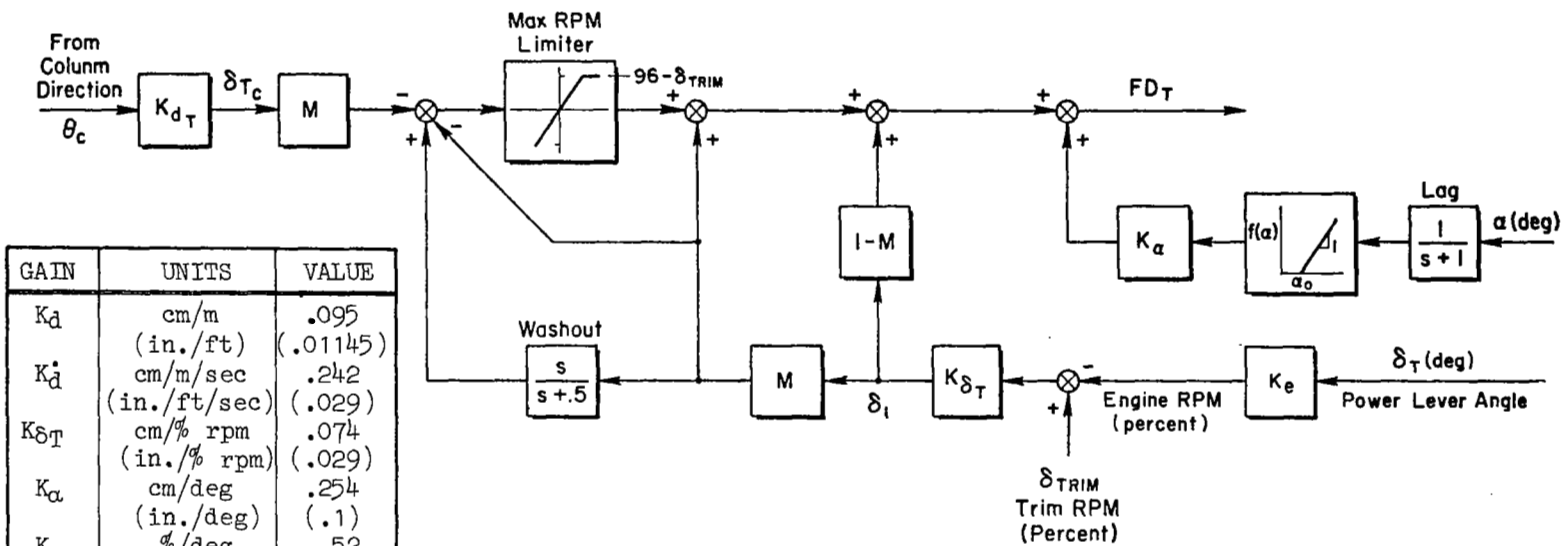

GAIN	UNITS	VALUE
K_d	cm/m (in./ft)	.095 (.01145)
$K_{\dot{d}}$	cm/m/sec (in./ft/sec)	.242 (.029)
$K_{\delta T}$	cm/% rpm (in./% rpm)	.074 (.029)
K_α	cm/deg (in./deg)	.254 (.1)
K_e	%/deg	.52
K_{d_T}	cm/cm (in./in.)	1.25 (1.25)

$$f(a) = \begin{cases} 0; \ \alpha < 10 \text{ deg} \\ (\alpha - 10); \ a \geq 10 \text{ deg} \end{cases}$$

$$\delta_{TRIM} = \begin{cases} 89\% \ V_{IAS} \geq 130 & M = 0 \ V_{IAS} > 80 \text{ kt} \\ 94\% \ V_{IAS} \leq 130; \ |d| > 30.5 \text{ m } (100 \text{ ft}) & M = 1 \ V_{IAS} < 79 \text{ kt} \\ 90\% \ |d| \leq 30.5 \text{ m } (100 \text{ ft}) & \text{(See Figure 4, Insert 3)} \end{cases}$$

Figure 16. Block Diagram for Thrust Flight Director

SECTION V

LATERAL FLIGHT DIRECTOR

Two competing lateral flight director systems evolved from the design effort. This section covers the details of the pilot/vehicle analysis procedures for each of the two competing systems.

A. DESIGN ANALYSIS PROCEDURE

A summary of the effect of the various feedbacks on the pilot/vehicle system requirements is given in Table 3. Early in the analysis, it was realized that two basic design concepts showed considerable promise. First, curved path tracking can be achieved by feeding forward certain trajectory-dependent parameters. This was named Flight Director A and represents a more conventional approach to the problem. A second, less conventional, approach was also developed which utilizes a washed-out bank angle feedback, thereby eliminating the need for trajectory-dependent feedforward signals. A generalized system for lateral control is shown in Fig. 17. The block diagram in Fig. 17 is based on the assumptions that: 1) the beam is range compensated; 2) all turns are coordinated; and 3) localizer noise is zero.

1. Dynamic Requirements

The closed-loop system response to a course command (y_c), initial condition offset, or a wind disturbance all depend on the characteristic equation of the closed-loop system which is given as:

$$\Delta_{CL} = \Delta + Y_p N_{\delta_W}^{\varphi}\left[G_\varphi + \frac{g}{s}\left(\frac{G_\psi}{U_o} + G_{\dot{y}}\right) + \frac{g}{s^2} G_y\right]$$

$$= \Delta + Y_p N_{\delta_W}^{FD} \qquad (11)$$

Closure of the flight director loop via Y_p (human or automatic pilot) drives the system poles into the flight director zeros, $N_{\delta_W}^{FD}$. These, in turn, are

TABLE 3. EFFECT OF FEEDBACKS ON SYSTEM REQUIREMENTS

FEEDBACKS	GUIDANCE AND CONTROL REQUIREMENTS		PILOT CENTERED REQUIREMENTS	
	PRIMARY REQUIREMENT	COMMENTS	PRIMARY REQUIREMENT	COMMENTS
Bank Angle, Φ	Stability	Requires feedforward for curved paths	Command bar consistency	Mid-frequency flight director motions should look like bank angle
Washed Out Bank Angle, φ	Stability	Washout time constant must be high enough to satisfy stability requirement yet low enough to insure good path following and disturbance regulation characteristics	Command bar consistency	Mid-frequency flight director motions should look like bank angle Washout must be high enough to maintain face validity
Roll Rate, p	None	Tends to reduce path damping	Minimum pilot compensation Remnant suppression	Provides K/s-like response at frequencies beyond the roll mode Provides good flight director response at curved path intercept point
Heading, ψ	Path Damping	Requires feedforward for curved path and for disturbance regulation on curved path — not practical	Minimum pilot compensation Path mode consistency Remnant suppression	Determines localizer capture rate
Washed Out Heading, ψ_w	Path Damping	Requires feedforward for curved path and wind shear on straight path	Same as above	Same as above
Course Angle, χ	Path Damping	Requires feedforward for curved path Requires inertial navigation system or equivalent for measurement	Same as above	Same as above
Crosstrack Rate, $\dot{y}$	Path Damping	Does not require feedforward Beam noise problems due to differentiation of crosstrack deviation	Same as above	Same as above
Crosstrack Error, y_c	Path Command and Disturbance Regulation		Path mode consistency	Should be compatable with localizer errors High sensitivity at long distances from touchdown are not desirable
Localizer Error, ϵ	Path Command and Disturbance Regulation	Stability problems due to constantly varying crosstrack deviation sensitivity with range	Same as above	
Beam Integral	Disturbance Regulation	Long time constant required for stability reduces regulation effectiveness	Same as above	Results in inconsistencies between command and localizer errors after periods of unattended operation

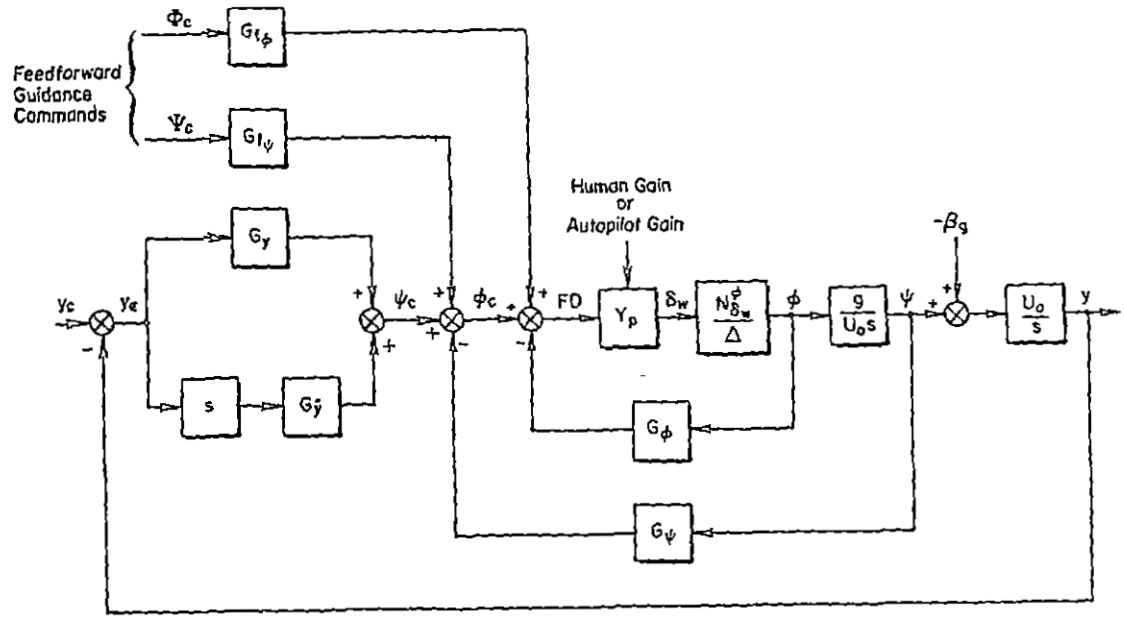

Figure 17. General Block Diagram for Lateral Flight Director

defined by the selection, shaping, and relative weighting of the feedbacks and feedforwards, G_i. $N^{\Phi}_{\delta_W}$ and Δ in Eq. 11 represent the roll numerator and characteristic equation of the augmented airplane which generally has the following form:

$$\frac{N^{\Phi}_{\delta_W}}{\Delta} = \frac{L_{\delta_{W_{aug}}}}{s(s + 1/T_{R_{aug}})} \tag{12}$$

Generically, the dominant roots of the augmented airplane consist of a roll subsidence mode and a spiral mode at (or near) the origin. The open-loop transfer function which defines the effective controlled element of the flight director to wheel response is obtained from Fig. 17 and Eqs. 11 and 12 as follows:

$$\frac{FD}{\delta_W} = \frac{L_{\delta_{W_{aug}}}\left[s^2 G_\varphi + gs(G_\psi/U_o + G_{\dot{y}}) + gG_y\right]}{s^3(s + 1/T_{R_{aug}})} \tag{13}$$

The generic root locus and Bode (frequency) characteristics which illustrate the effects of a typical piloted closure of the flight director loop are given in Fig. 18. From Fig. 18 it can be seen that the characteristic modes of the closed-loop system may be optimized by adjusting the numerator coefficients (feedback transfer functions) in Eq. 13. The following guidance and control requirements result directly from these considerations.

a. The numerator must be at least a second order at frequencies well below the roll mode ($\omega_D << 1/T_R$) for system stability and to maximize the region of K/s. Among other things, this implies $G_\Phi \neq 0$.

b. Heading feedback, G_ψ, and/or beam rate feedback, $G_{\dot{y}}$, is necessary for system damping. Note that beam rate feedback implies differentiation of beam error, y_ϵ.

c. The frequency of the $N^{FD}_{\delta_w}$ numerator zeros (ω_D) determines the maximum achievable bandwidth of the closed-loop system. As such, it must be large enough to allow good command following and disturbance regulation.

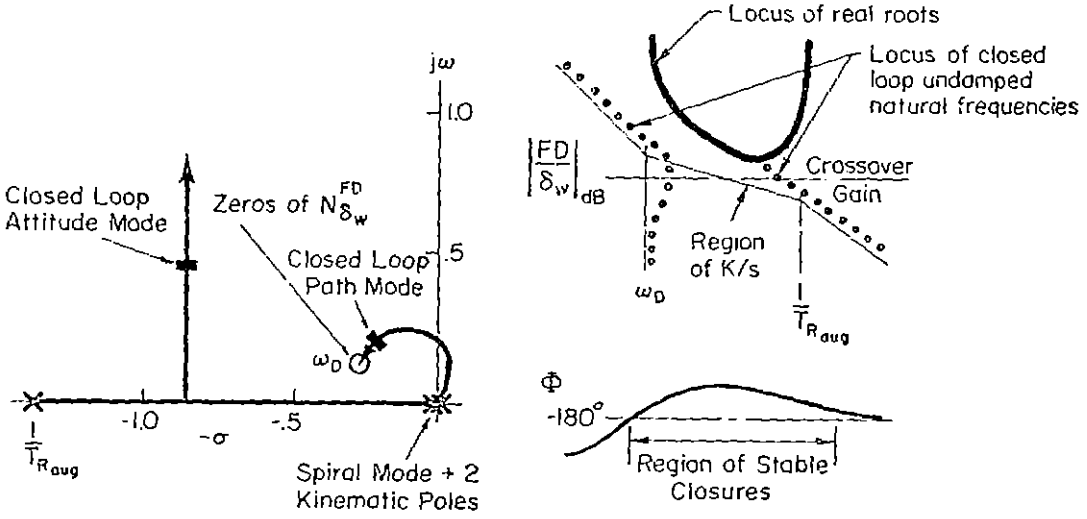

Figure 18. Generic System Survey of Piloted or Automatic System Closure of Lateral Flight Director Loop

The underlined words refer to specific requirements listed in Table 1. Note that Requirements a and c above are in conflict and involve a fundamental tradeoff between command following/disturbance regulation and system stability.

2. Steady-State Requirements

The above analysis lends certain insights as to the necessary form of the feedbacks to obtain desirable system dynamic response. To complete the picture, we shall now consider the steady-state requirements. These relate to various levels of command following (straight and curved courses) and disturbance regulation (wind and wind shear). This is accomplished by writing the differential equation for the closed-loop system from the block diagram in Fig. 17 in terms of the beam error y_ϵ and solving for the steady-state response to y_c and v_g by use of the final value theorem. The differential equation is given in Laplace transform style as:

$$\left[s^2 + \frac{g}{G_\varphi}\left(\frac{G_\psi}{U_o} + G_{\dot{y}}\right)s + \frac{g}{G_\varphi}G_y\right]y_\epsilon = s\left[s + \frac{g}{G_\varphi}\left(\frac{G_\psi}{U_o} + G_{\dot{y}}\right)\right]y_c + \left(s + \frac{G_\psi}{G_\varphi}\frac{g}{U_o}\right)v_g \qquad (14)$$

This equation is based on the assumption that the flight director loop is closed tightly so that $\varphi/\varphi_c \doteq 1/G_\varphi$ and that the feedforward operator $G_i = 0$.

Each of the feedback transfer function blocks (G's) may assume three possible forms in order to comply with the requirements stated above. The first has a free s in the denominator, such as $G_y = K_y + (K_{\bar{y}})/s = (K_y s + K_{\bar{y}})/s$; the second has a free s in the numerator (e.g., $G_\varphi = sK_\varphi$); and the last represents just a pure gain feedback. It can be assumed that G_φ and G_ψ would not contain a denominator free s (integral equalization) since this could force a localizer standoff. Therefore, the practical guidance and control possibilities for all three flight director feedbacks are constant or washed-out roll angle, constant or washed-out heading, and beam error or beam error plus integrated beam error. Thus,

$$
\begin{aligned}
G_{\varphi} &= k_{\varphi} \quad \text{or} \quad sk_{\varphi} \\
G_{\psi} &= k_{\psi} \quad \text{or} \quad sk_{\psi} \\
G_{y} &= k_{y} \quad \text{or} \quad k_{\bar{y}}/s \\
G_{\dot{y}} &= k_{\dot{y}}
\end{aligned}
\tag{15}
$$

Table 4 show the magnitude of the steady-state beam error to three orders of beam command, i.e., step, ramp, and parabola, and two wind inputs, i.e., constant crosswind and crosswind shear, as a function of various combinations of feedback equalization. For example, Line 3 shows that pure gain feedbacks of bank angle, heading, and localizer deviation would produce

TABLE 4

STEADY-STATE ERRORS

FEEDBACKS				STEADY STATE ERROR		
G_{φ}	G_{ψ}	$G_{\dot{y}}$	G_{y}	TO STEP BEAM	TO STEP v_g OR DUAL ANGLE BEAM	TO v_g SHEAR OR CURVED PATH
					PATH DAMPING WITH HEADING	
k_{φ}	sk_{ψ}	0	$k_y + \frac{k_{\bar{y}}}{s}$	0	0	0
k_{φ}	sk_{ψ}	0	k_y	0	0	OFFSET
k_{φ}	k_{ψ}	0	k_y	0	OFFSET	∞
k_{φ}	k_{ψ}	0	$k_y + \frac{k_{\bar{y}}}{s}$	0	0	OFFSET
					PATH DAMPING WITH BEAM RATE	
sk_{φ}	0	$k_{\dot{y}}$	$k_{y_{k_{\bar{y}}}}$	0	0	0
sk_{φ}	0	$k_{\dot{y}}$	$k_y + \frac{k_{\bar{y}}}{s}$	0	0	0
k_{φ}	0	$k_{\dot{y}}$	$k_{y_{k_{\bar{y}}}}$	0	0	OFFSET
k_{φ}	0	$k_{\dot{y}}$	$k_y + \frac{k_{\bar{y}}}{s}$	0	0	0

NOTE: sk_{φ}, sk_{ψ} represent washout equalization

$k_{\dot{y}}$ represents beam rate

$k_{\bar{y}}/s$ represents beam integral

No s represents a finite, non-zero gain at DC

no error to a step beam command (such as would appear for engagement), a constant error to a steady crosswind or ramp change in beam angle, and an ever-increasing error to a crosswind shear or curved path command. By washing out the heading feedback (Line 2) there is no steady-state error to a steady crosswind or ramp change in beam angle. This equalization is typically found in CTOL approach control systems.

Since wind shear and curved path approaches are much more pertinent to STOL aircraft, the more important conclusions to be drawn from Table 4 are as follows:

a. Without beam integral, beam rate ($k_{\dot{y}}s$), along with washed-out roll angle (Line 5) is the only set that has zero path error to curved paths and wind shears.

b. With beam integral it is not necessary to wash out roll attitude in order to assure zero error to curved paths and wind shears.

While beam integral appears attractive from a steady-state analysis standpoint, the values of the integral gain, $k_{\bar{y}}$, that can be achieved without degrading the system stability results in a very long path mode response. Thus, the fact that the steady-state error is mathematically zero is of little practical value. Two practical alternatives exist; one is to use washed-out bank angle and the other is to consider the addition of feedforward commands. Both alternatives were considered in the present design exercise, FD A with a feedforward and FD B with washed-out feedback. The characteristics of the feedforward required for the FD A concept are discussed in the following subsection.

3. Feedforward Guidance Commands (FD A)

In essence, the guidance and control requirements for command following and disturbance regulation in the lateral flight director are satisfied via the outer loop (crosstrack deviation). Other requirements, such as stability and damping, necessitate the use of inner loops which tend to complicate matters when following curved paths or regulating against wind and wind shear. In these situations the steady-state inner-loop feedbacks are not nominally zero, resulting in standoffs with the crosstrack error signal, y_ϵ.

Consider again the generalized lateral flight director block diagram in Fig. 17. If the pilots keeps the flight director centered ($FD_w = 0$), the control law which is automatically satisfied becomes:

$$FD_w = -G_\varphi\varphi - G_\psi\psi + G_y y_\epsilon + G_{f_\varphi}\Phi_c + G_{f_\psi}\Psi_c \tag{16}$$

where Φ_c and Ψ_c are the feedforward guidance command variables to be later defined. In the absence of feedforward guidance commands, the crosstrack deviation may be written as:

$$y_\epsilon = \frac{1}{G_y}(G_\varphi\varphi + G_\psi\psi) \tag{17}$$

Note that the desired result is always to make $y_\epsilon = 0$ and that this will only occur if the bank angle, φ, and heading, ψ, are nominally equal to zero when tracking the desired course. This, of course, is only true for straight paths in the absence of crosswind and crosswind shear. Several ways of getting around this problem exist. One possibility is to wash out φ and ψ via the feedback transfer functions, G_φ and G_ψ. A second possibility is to add a parallel integrator to G_y. This is impractical for reasons previously discussed. Finally, we can develop feedforward guidance commands for each of the feedback variables resulting in the following control law (see Fig. 17):

$$FD_w = G_\varphi(\Phi_c - \varphi) + G_\psi(\Psi_c - \psi) + G_y y_\epsilon \tag{18}$$

where $G_{f_\varphi} = G_\varphi$ and $G_{f_\psi} = G_\psi$. The complexity of the command signals will depend on the shape of the desired course and the nature of the wind disturbance.

Clearly, it is desirable to select inner-loop feedbacks which minimize the complexity of the corresponding feedforward commands. Because of the rapidly changing heading during a turn and the sensitivity of the required heading to crosswinds, it is not practical to use heading for path damping on a curved path. The same argument holds true for the lateral course

angle, λ. For this reason, crosstrack rate, $\dot{y}$, has been selected to provide the primary path damping. Note that $\dot{y}$ is nominally zero for all paths and wind conditions and therefore does not require a feedforward command signal.

The bank angle feedforward guidance command is based on nulling the crosstrack acceleration, $\ddot{R}$, for a given turn radius, R_c. These are related as follows:

$$\ddot{R} = \frac{V_{GS}^2}{R_c} - g \tan \varphi \tag{19}$$

It follows that the command bank angle should be:

$$\Phi_c = \tan^{-1} \frac{V_{GS}^2}{R_c g} \tag{20}$$

The flight director Eq. 16 now becomes:

$$FD_W = G_\varphi \left(\tan^{-1} \frac{V_{GS}^2}{R_c g} - \varphi \right) + G_y y_\epsilon = 0 \tag{21}$$

Elimination of standoffs in y_ϵ depend upon the following considerations:

a. R_c must be the exact turn radius consistent with the error signal, y_ϵ.

b. Accurate measurement of ground speed is necessary.

c. Accurate measurement of bank angle is required.

The bank angle command defined by Eq. 20 only accounts for wind in the sense that ground speed changes in a turn. The bank angle command for zero steady-state error in the presence of wind and wind shear has been derived in Ref. 13 and is given as:

$$\Phi_c = \tan^{-1} \frac{V_{GS}^2}{R_c g} - \frac{1}{g} \frac{dv_g}{dt} \tag{22}$$

where v_g is the component of wind perpendicular to the airspeed vector. Expanding this into inertially fixed X and Y coordinates yields:

$$\Phi_c = \tan^{-1} \frac{V_{GS}^2}{R_c g} - \frac{1}{g}[\dot{V}_{WY} \cos \psi - \dot{V}_{WX} \sin \psi - V_{WY} \sin \psi\dot{\psi} - V_{WX} \cos \psi\dot{\psi}] \qquad (23)$$

A sketch of the geometry defining the wind coordinates is given below.

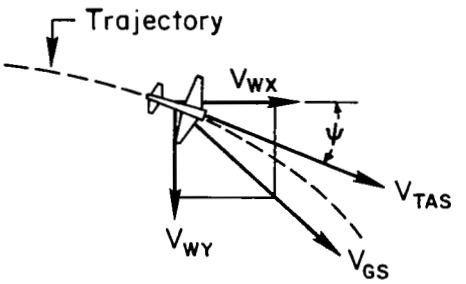

This form of bank angle command is somewhat impractical due to the requirement for continuous measurement of wind and wind shear. Furthermore, simulator results for curved path tracking in the presence of wind and wind shear indicated that crosstrack errors were negligible using the simplified Φ_c in Eq. 21.

4. Derived Beam Rate

The practical difficulties associated with using beam rate for path damping involve considerations of beam noise. A conventional circuit for obtaining derived beam rate ($\dot{y}_D$) from the localizer error (y_ϵ) is shown in Fig. 19. The transfer function for the portion of the flight director command due to the summation of beam error and beam rate (φ_{c_1} in Fig. 19) is given as:

$$\frac{\varphi_{c_1}}{y_\epsilon} = \frac{(K_y + \frac{1}{\tau} K_{\dot{y}}^{\cdot\cdot})\left(s + \frac{K_y}{K_y\tau + K_{\dot{y}}^{\cdot}}\right)}{(s + 1/\tau)} \qquad (24)$$

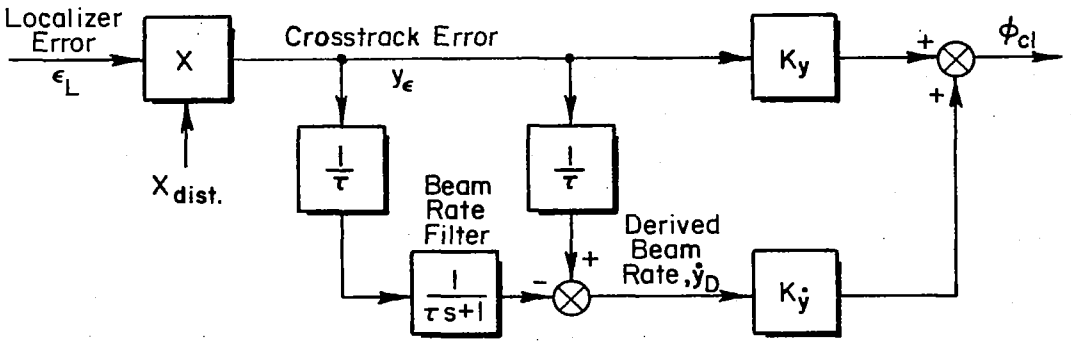

Figure 19. Block Diagram of Circuit for Derived Beam Rate

The derived beam rate, $\dot{y}_D$, is given as:

$$\dot{y}_D = \frac{s}{\tau s + 1} y_\epsilon \tag{25}$$

An indication of the beam noise characteristics which will be seen on the flight director can be obtained by consideration of rms values of φ_{c_1} for a given power spectral density function, $\Phi(\omega)$, of the localizer signal. A plot of the average power spectral density of nine directional localizers was obtained in Ref. 12 and is given in Fig. 20. Using the fit shown in Fig. 20, the rms values of φ_{c_1} may be computed given an rms localizer noise:

$$\sigma^2 = 2 \int_0^\infty \Phi(\omega)\, d\omega \tag{26}$$

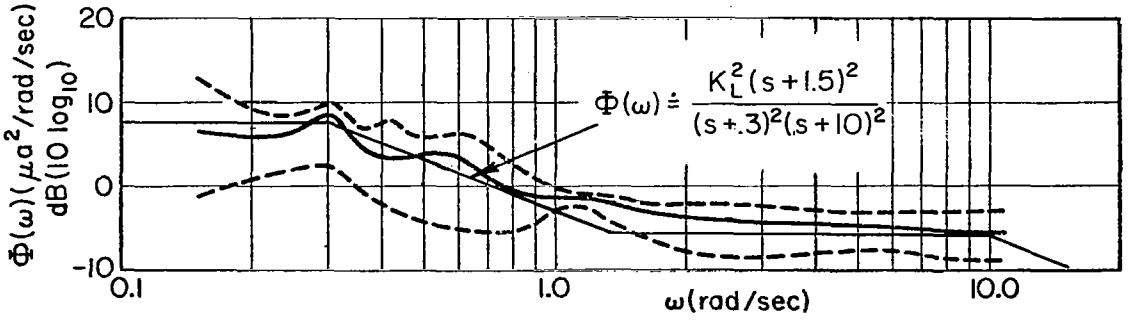

Figure 20. Average Directional Localizer Power Spectral Density

and adjusting the gain, K_L, appropriately. From Ref. 14 the mean-square values of localizer noise varied from 1.48μa to 6.92μa over 12 localizers. Converting μa to degress of localizer error and picking 4μa as a representative value, the rms localizer error is given as 0.066 degrees.* The resulting rms flight director noise is given as a function of beam rate filter time constant, τ, and range from touchdown, X_{dist}, in Fig. 21.

As would be expected, increasing the beam rate filter time constant reduces the flight director noise. However, from Eq. 25 the derived beam rate is restricted to frequencies below $1/\tau$ resulting in decreased stability at the path mode frequency, ω_D, as $1/\tau$ approaches ω_D. While these results are for a conventional localizer, they are conservative in that the MLS systems are typically of a lower noise content.

The beam rate noise filter time constant was taken to be 4 sec to minimize the beam noise input to the flight director. This results in elimination of derived beam rate near the path mode frequency ($1/\tau \doteq \omega_p$) with a concomitant reduction in path mode damping to an unacceptable level ($\zeta_D = 0.08$). Complementary filtering to obtain "beam rate" at frequencies greater than $1/\tau$

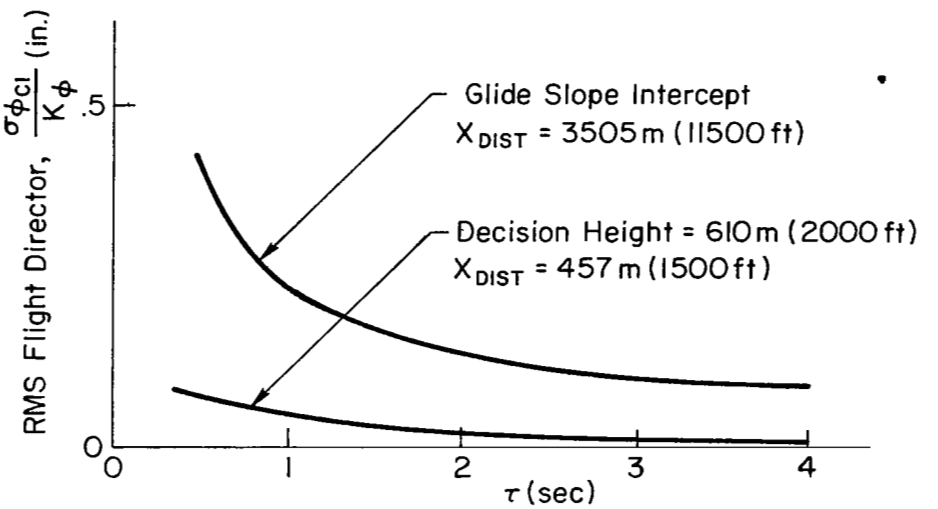

Figure 21. RMS Flight Director Signals Due to Conventional Localizer Noise

*This assumes a standard localizer width of ±2.5 deg and ±15μa full scale.

is accomplished by using bank angle and body-fixed lateral acceleration to generate a roll-stabilized lateral acceleration term which is passed through a low pass filter.

The lateral acceleration relative to a nominal curved path may be approximated by:

$$\Delta\ddot{y} = a_{y_{MEAS}} + g \cos\theta(\varphi - \varphi_c) \qquad (27)$$

where $\varphi_c = \tan^{-1} V_{GS}^2/Rg$ defines a commanded circular path radius R_c (see Eq. 21). This expression, when passed through a first-order low pass filter with time constant, τ, gives $\Delta\dot{y}$ at frequencies greater than $1/\tau$. The final mechanization of the derived beam rate ($\dot{y}_D$) is given in Fig. 22.

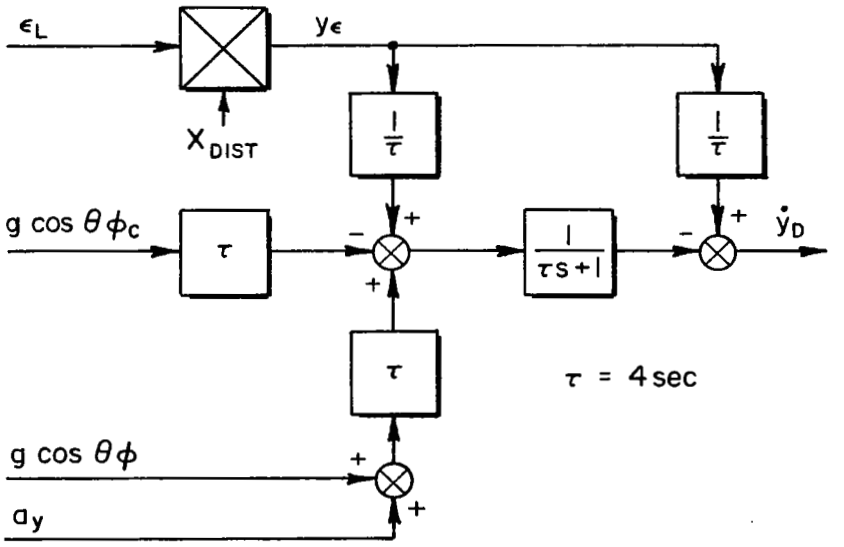

Figure 22. Complementary Filter for Derived Beam Rate on a Curved Path

B. PARAMETER ADJUSTMENT ANALYSIS (FD A)

The analytical design procedure utilized to set the final system gains and feedback transfer functions and limiters was formulated so that the system requirements in Section II could be interpreted directly in terms of certain quantitative criteria. The system requirements and corresponding analytical measures are summarized in Table 5. The procedures implicit in the Table 5 requirements are used to develop and validate FD A in this subsection and FD B in Subsection C.

TABLE 5

RELATIONSHIP BETWEEN ANALYTICAL PERFORMANCE MEASURES AND PILOT/VEHICLE REQUIREMENTS

ANALYTICAL MEASURE	PILOT/VEHICLE REQUIREMENTS (SECTION II)
Root locus of piloted closure of the effective controlled element, FD/δ_W	● Stability and damping ● Response quality (modal interactions)
Frequency response (Bode plot) of FD/δ_W	● K/s near crossover for 1) Minimum pilot compensation 2) Insensitivity to pilot response variations 3) Remnant suppression ● Stability and damping
Time response to initial condition offset	● Response quality (path mode consistency)
Time response to initial condition offset with crosswinds and response to wind shear	● Disturbance regulation ● Response quality (face validity)
Time response to path command input (circular path)	● Command following

A block diagram which incorporates the feedbacks, feedforward, and complementary filter discussed previously for the FD A concept is given in Fig. 23. Also included in this final system block diagram are:

- The final gains and time constants utilized for the example Augmentor Wing aircraft.

- A bank angle limiter to eliminate the possibility of commanding excessive bank angles (set to 30 deg based on pilot commentary).

- A course rate limiter to preclude the possibility of commanding large rapid bank angles if the aircraft is significantly off course. This limiter was set as a function of groundspeed so as to achieve a 20 deg re-intercept as follows:

$$|\dot{y}_{lim}| = \frac{K_{\dot{y}}}{K_y}\dot{y} = \frac{K_{\dot{y}}}{K_y} V_{GS} \sin 20^o$$

- Feedforward shaping filters to eliminate step-like command bar motions in response to the step Φ_c that occurs Δt sec before course intercept. It was originally thought that the command bar motions should occur at a rate below the pilot's tracking frequency. This would allow the pilot to keep the command bar centered at all times. As it turned out, the shaping required to achieve this result gives an erroneous Φ_{co} at path mode frequencies resulting in a standoff in crosstrack deviation. In addition, the pilots did not object to a discrete flight director command as it tended to serve as status information with regard to a change in course geometry. The pilot opinion was very sensitive to his ability to recenter the bar without overshoots or unduly large control inputs. Setting $\tau_A = \tau_B = 0$ was found to be undesirable because it was difficult to tell how much δ_w was required to get the command bar off the limit, and because of the very abrupt nature of the command. As a final compromise, the lag time constants were set to unity ($\tau_A = \tau_B = 1.0$). This resulted in relatively smooth command bar motions and did not affect the course tracking accuracy, i.e., the requirements for face validity and path mode consistency were both satisfied.

- A feedforward initiation time increment (note in upper left corner) to initiate the bank angle command Δt seconds before curved/straight course transitions. Variations of Δt_1 and Δt_2 during the piloted simulation showed that the transition characteristics are quite sensitive to these parameters. The curved to straight transition (Δt_2) exhibited the greatest sensitivity because the aircraft would be turned on to the straight localizer at the wrong heading as Δt_2 was varied away from its "optimum value." The ensuing bank angle reversals

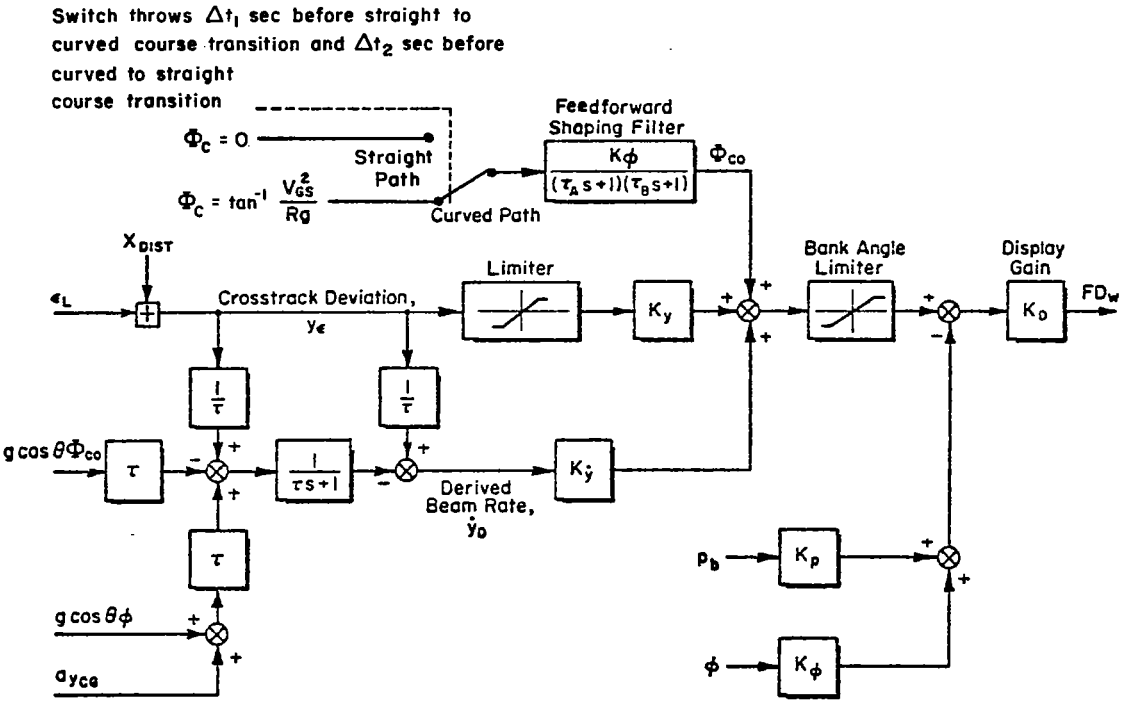

CONSTANTS	UNITS	VALUE
K_y	rad/m (rad/ft)	.0066 (0.002)
$K_{\dot{y}}$	rad/m/sec (rad/ft/sec)	.054 (0.0165)
K_ϕ	—	1.6
K_p	sec	1.3
K_D	cm/rad (in./rad)	2.54 (1.0)
τ_A	sec	1.0
τ_B	sec	1.0
τ	sec	4.0
$\Delta t_{1,2}$	sec	3.0
M	—	+1 right turns −1 left turns
y_{LIM}	m (ft)	.854 V_{GS} (2.8) V_{GS}
Φ_{LIM}	rad	0.524

Figure 23. Block Diagram and Constants for Flight Director A

resulted in considerably degraded pilot opinion. Once Δt_2 was set at the "proper value" (3 sec), the straight localizer intercept was very smooth. The optimum value for $\Delta t_{1,2}$ is insensitive to variations in aircraft speed, course radius, and winds. This results in a desirable system simplification in that $\Delta t_{1,2}$ can be set to a constant without compromise in system performance throughout the flight envelope.

The flight director to δ_w input transfer function corresponding to the block diagram in Fig. 23 is given as:

$$N_{\delta_w}^{FD} = \frac{K_p K_D L_{\delta_w}}{s^2}\left[s^3 + \frac{K_\varphi}{K_p}s^2 + g\frac{K_{\dot{y}}}{K_p}s + g\frac{K_y}{K_p}\right] \qquad (28)$$

The zeros of this numerator represent the limiting characteristics of the system closed-loop modes as the pilot increases his gain on the FD_w/δ_w closure. Comparison of Eq. 28 with Eq. 13 reveals that the addition of roll rate feedback, i.e., $G_\varphi = K_\varphi + K_p s$, increases the order of $N_{\delta_w}^{FD}$ from two to three, making the effective controlled element $(N_{\delta_w}^{FD}/\Delta)$ K/s-like out to infinite frequency. The coefficients of Eq. 28 were adjusted in accordance with the pilot/vehicle requirements discussed in Section II, resulting in the system survey shown in Fig. 24. This is valid for all flight conditions because the augmented lateral airplane transfer function was essentially invariant with speed.

The root locus in Fig. 24 indicates that the dominant system response is third order with the second-order closed-loop flight director mode, ω_{FD}', occurring at slightly higher frequency than the first-order subsidence, $1/T_{FD}'$, in the region of crossover. The gain crossover region was estimated from the results of several simulator programs, resulting in the closed-loop modes shown. One of the primary goals in the design was to make the effective controlled element, FD/δ_w, K/s-like over a broad range of frequencies, and this is reflected in the Bode amplitude plot. The postulated crossover is in the K/s region and very near the frequency for maximum phase margin. Notice that deviations in pilot gain from the (assumed) nominal by, say, ±6 dB do not greatly affect the resulting closed-loop modes (see Bode).

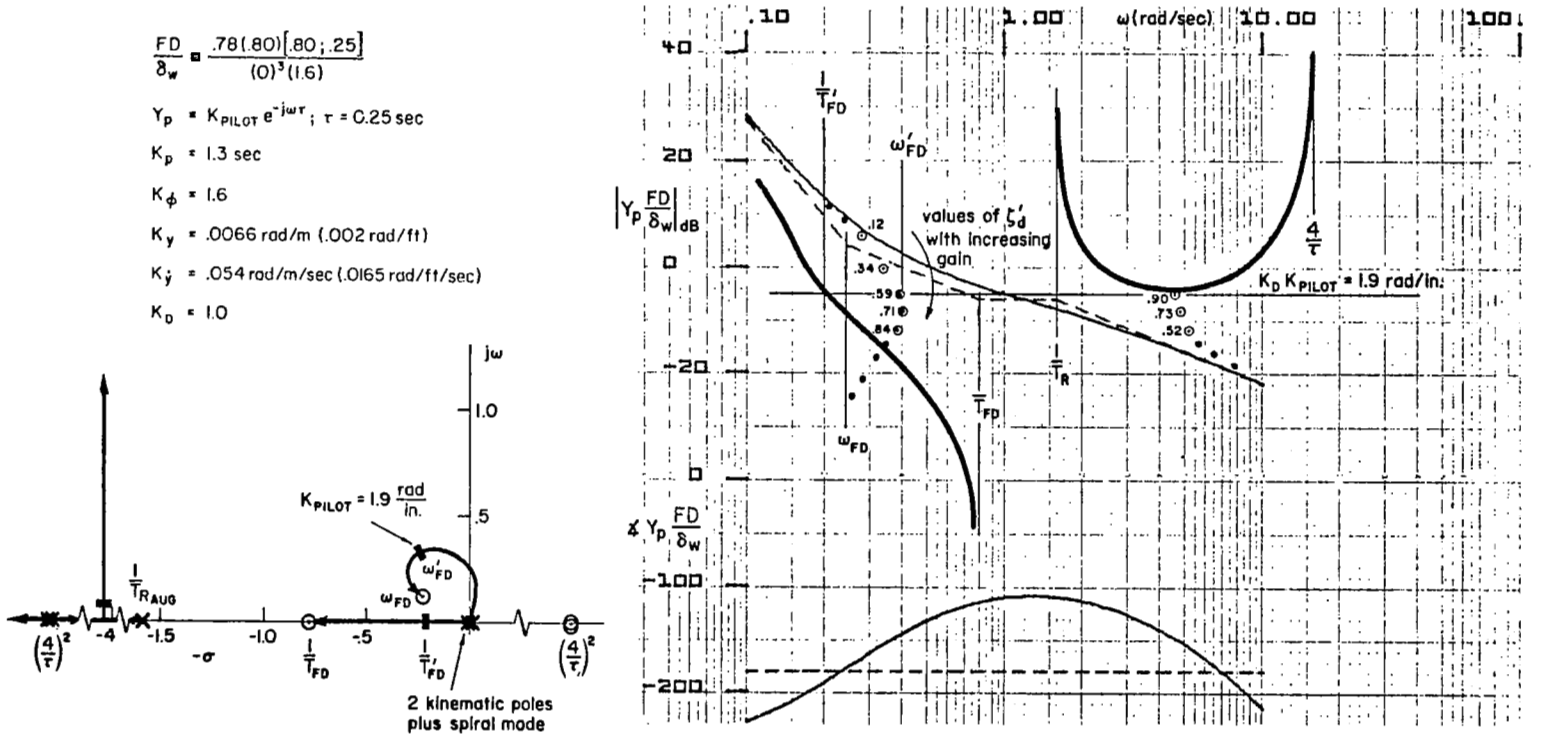

Figure 24. System Survey for Flight Director A, $Y_p(FD/\delta_w)$

Some concern was expressed initially over the unstable nature of the flight director at low frequency (see Fig. 24 root locus near the origin) and the effect this might have during periods of unattended operation. However, this was not a problem, and the pilots were totally unaware of any conditional stability aspects of the flight director.

The third-order nature of the response (two modes at nearly the same frequency) required close consideration of the response qualities requirement discussed in Section II. Increasing the rate gain, $K_{\dot{y}}$, tends to drive $1/T'_{FD}$ towards the origin, resulting in a higher-order-looking response. This is characterized by a localizer bug that initially moves toward the center and then seems to stand off.

The system was checked for disturbance regulation by looking at the time response to a crosswind and crosswind shear using a simplified digital simulation of the closed-loop airplane/display/pilot system. The results for positive and negative crosswinds of 25 kt for an initial condition offset of 122 m (400 ft) are shown in Fig. 25.* In both cases the disturbance regulation characteristics are seen to be quite good in that the aircraft is on course with an established crab angle within 20 sec. In the case of the left crosswind, the bank angle limiter is saturated until course convergence is established, resulting in a discontinuity in the flight director signal at about 5 seconds as the signal comes off the limiter. What this amounts to is a sudden change in the effective flight director law from $FD_w = (\varphi_{lim} - \varphi)$ to $FD_w = f(y_\epsilon, \dot{y}_D, \varphi, p)$. While this violates the pilot-centered requirements for "face validity," it is difficult to avoid since the bank angle limiter is necessary to satisfy other pilot-centered requirements. Results obtained during the piloted simulation indicated that this problem only occurred after a large abuse and was not objectionable enough to downrate the system. (Note that flying a heading parallel to the localizer with a 122 m (400 ft) offset in a 25 kt crosswind is a significant abuse of the system.)

*These and subsequent time histories were obtained from a simplified digital simulation described in Ref. 11.

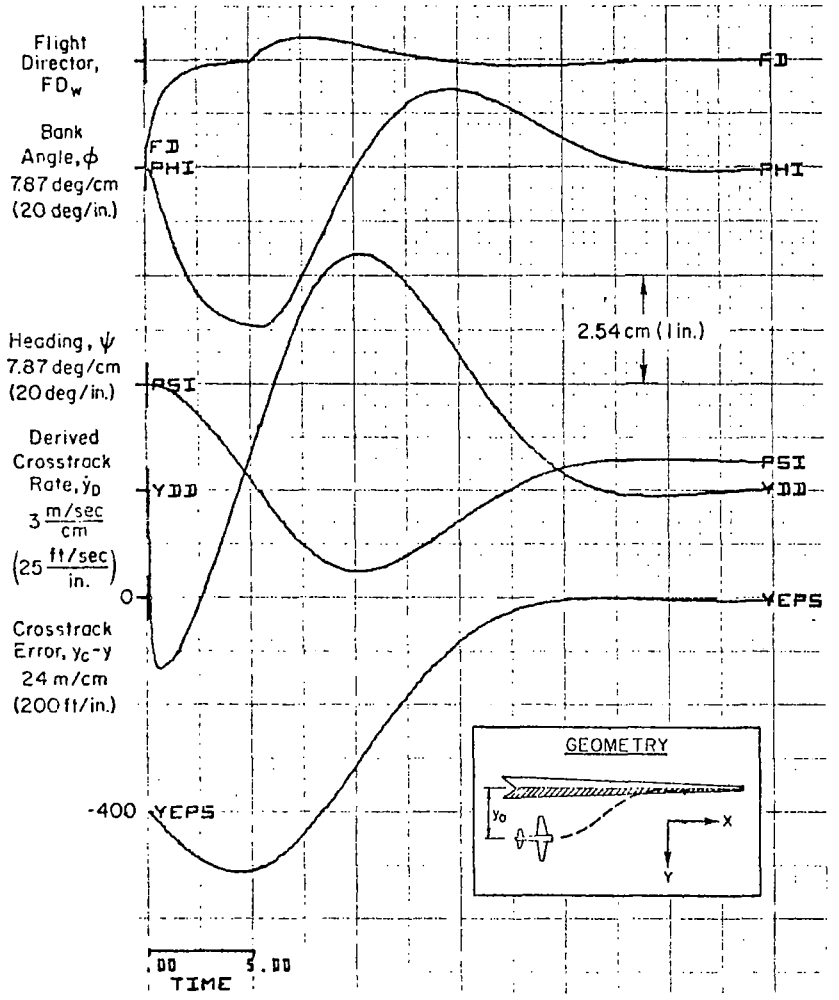

a) Crosswind From Left

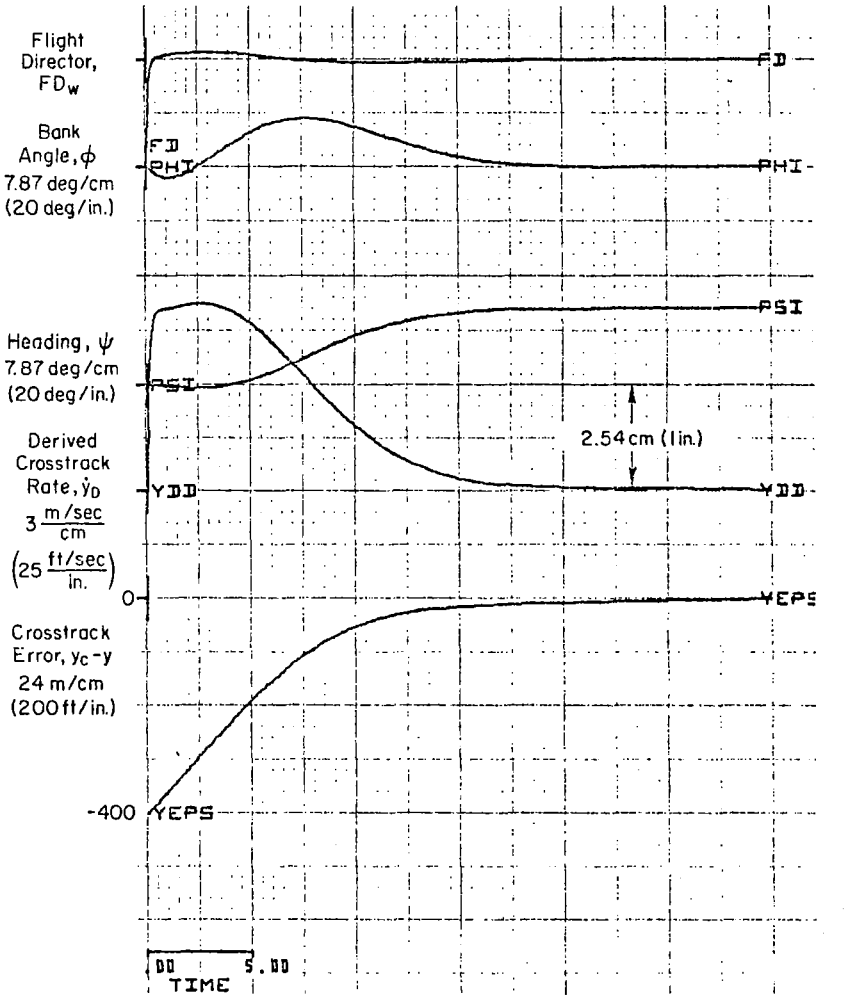

b) Crosswind From Right

Figure 25. Flight Director A Response to Initial Condition Offset with a 25 kt Crosswind at an IAS of 90 kt

From Table 4 (Line 7) we would expect to find steady-state offset to a wind shear input; more specifically, applying the final-value theorem to Eq. 14 for a gust ramp given by $\dot{v}_g/s^2$,

$$y_{\epsilon ss} = \frac{\dot{v}_g K_\varphi}{g K_y} = 25\ \dot{v}_g \tag{29}$$

Wind shear is usually given as a gradient with respect to altitude. Assuming a speed of 60 kt on a −7.5 deg glide slope, 10 kt/30 m (100 ft) (a strong shear) is equivalent to .68 m/sec^2 (2.23 ft/sec^2), which would result in a standoff of 17 m (56 ft) during the shear.

C. ERROR ANALYSIS FOR FD A

The feedforward bank angle command and the feedback bank angle signal are subject to measurement errors which arise from errors in the measured groundspeed and vertical gyro precession in a turn. An important figure of merit of the lateral flight director system is the sensitivity of crosstrack standoffs due to these measurement errors. Ignoring the crosstrack rate and roll rate feedbacks which have no effect on trajectory standoffs, the flight director equation may be derived from Fig. 23 as follows:

$$K_y y_\epsilon + K'_\varphi(\Phi_c - \varphi_M) = FD_w \tag{30}$$

where

$K'_\varphi = K_\varphi + g\tau K_{\dot{y}}$

$\Phi_c \doteq V_{GS_M}^2/R_c g$, commanded bank angle based on measured groundspeed, V_M

$\varphi_M = \varphi + \varphi_{BIAS}$, measured bank angle

$y_\epsilon = R - R_c$, crosstrack error or difference between the actual radius, R, and the commanded radius, R_c

Noting that $\varphi \doteq V_{GS}/Rg$, Eq. 21 can be rewritten in terms of the measured and actual groundspeeds and the bank angle bias as follows:

$$K_y y_\epsilon + K'_\varphi \left[\frac{V^2_{GS_M}}{R_c g} - \frac{V^2_{GS}}{(R_c + y_\epsilon)g} - \varphi_{BIAS} \right] = FD_w$$

Assuming the flight director is kept centered ($FD_w = 0$) and that $y_\epsilon << R_c$*, the sensitivity coefficients of crosstrack error to bank angle and groundspeed measurement errors are given as follows:

$$\frac{\partial y_\epsilon}{\partial \varphi_{BIAS}} = \frac{1}{(K_y/K'_\varphi) + (V^2_{GS}/R^2_c g)} \tag{31}$$

$$\frac{\partial y_\epsilon}{\partial \Delta V} = \frac{2V_{GS}}{R_c g[(K_y/K'_\varphi) - (V^2_{GS}/R^2_c g)]} \tag{32}$$

where ΔV represents the groundspeed measurement error ($V_{GS_M} - V_{GS}$). These sensitivities are plotted in Fig. 26 as a function of groundspeed and turn radius. The crosstrack errors for practical values of ΔV and φ_{BIAS} are

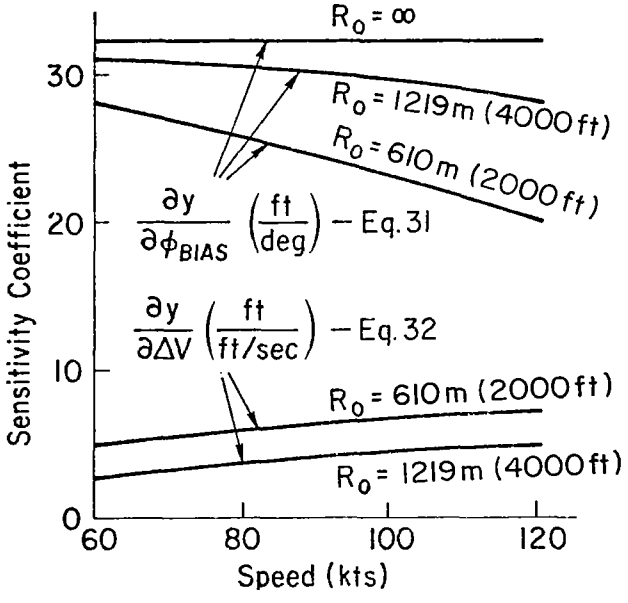

Figure 26. Crosstrack Error Sensitivities, FD A

*If $y_\epsilon << R_c$, $1/(R_c + y_\epsilon) \doteq (1/R_c)[1 - (y_\epsilon/R_c)]$.

seen to be quite small. As a check on the analysis, a φ_{BIAS} of 5 deg was input on the FSAA simulator. The computed crosstrack standoff from Fig. 26 was in excellent agreement with the simulation 38 m (125 ft).

D. PARAMETER ADJUSTMENT ANALYSIS (FD B)

Flight Director B represents a somewhat more novel approach to the problem in that it does not require feedforward signals and will track any arbitrary path without external inputs. As such, the design is less straightforward than FD A, requiring additional tradeoffs and in some cases compromises in performance. As will be shown, the system limitations are of practical interest only when a small turn radius is required (R_c < 1219 m (4000 ft). For such cases, a washed-out step bank angle command must be added to allow the aircraft to "blend in" to the curved path prior to reaching the point of tangency. A block diagram of FD B which reflects the feedback structure and final system constants used for the Augmentor Wing STOL is given in Fig. 27.

From Fig. 27 the flight director to wheel numerator is given as:

$$N_{\delta_w}^{FD} = \frac{K_D L \delta_w}{s^2\left(s + \frac{1}{T_{wo}}\right)\left(s + \frac{1}{\tau}\right)} \left\{ K_p s^5 + \left[K_p\left(\frac{1}{T_{wo}} + \frac{1}{\tau}\right) + K_\varphi \right] s^4 + \left(\frac{K_\varphi}{\tau} + \frac{K_p}{T_{wo}\tau}\right) s^3 \right.$$

$$\left. + g\left(\frac{K_{\dot{y}}}{\tau} + K_y\right) s^2 + g\left[\frac{K_{\dot{y}}}{\tau T_{wo}} + K_y\left(\frac{1}{T_{wo}} + \frac{1}{\tau}\right)\right] s + \frac{g K_y}{T_{wo}\tau} \right\} \quad (33)$$

The increase from a third-order numerator (FD A) to a fifth-order numerator is due to the bank angle washout circuit, and the lag at $1/\tau$ in $G_{\dot{y}}$ (see Eq. 25) required to filter beam noise. This lag is effectively eliminated in Flight Director A by complementary filtering (see Fig. 22). The design of Flight Director B is predicated on being able to follow any beam shape (within system limits) without prior knowledge of the beam geometry. Complementary filtering schemes require knowledge of the beam geometry and are therefore "not allowed" in the design of FD B. A key design tradeoff is to maximize the beam rate filter time constant, τ, to reduce system noise while maintaining the required stability characteristics.

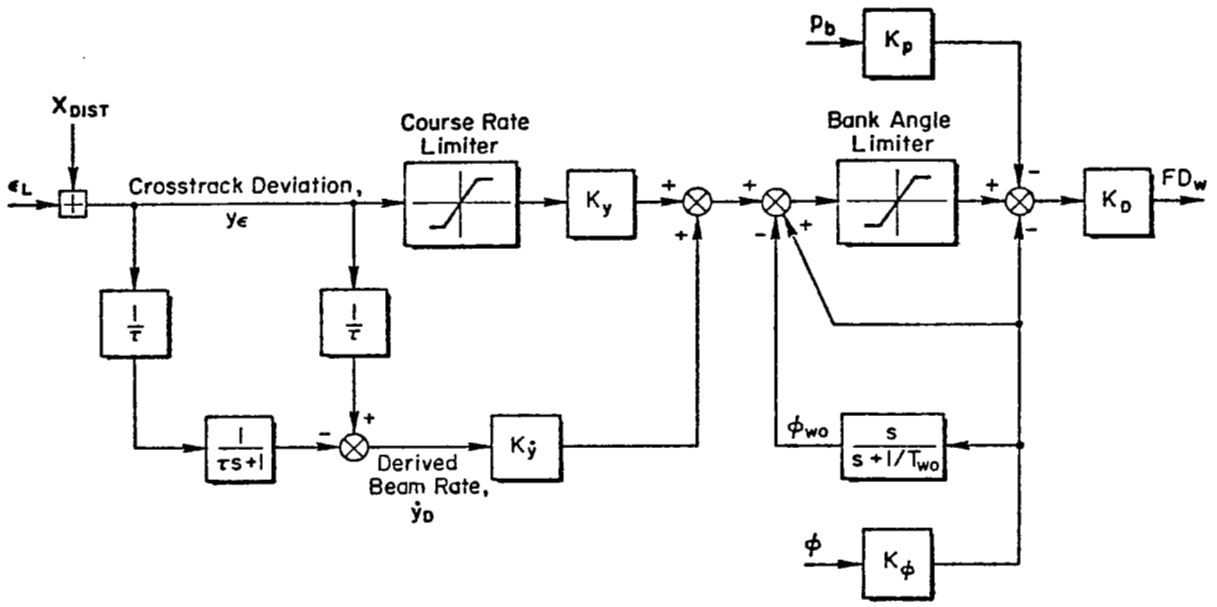

CONSTANTS	UNITS	VALUE
K_y	rad/m (rad/ft)	.0066 (.002)
$K_{\dot{y}}$	rad/m/sec (rad/ft/sec)	.054 (.0165)
K_ϕ	-	1.35
K_p	sec	.35
K_D	cm/rad (in./rad)	3.81 (1.5)
T_{wo}	sec	10.0
τ	sec	0.5
y_{LIM}	m (ft)	.854 V_{GS} (2.8) V_{GS}
ϕ_{LIM}	rad	.524

Figure 27. Block Diagram and Constants for Flight Director B

Preliminary adjustments of the system parameters were accomplished using root locus factoring techniques to determine the effects of the system parameters on the zeros of $N_{\delta_w}^{FD}$. The first step in this process was to set $K_p = 0$ and to factor Eq. 33 in terms of K_φ. The resulting equation takes on a relatively simple form as follows:

$$1 + \frac{g}{\tau}\frac{K_{\dot{y}}}{K_\varphi}\frac{(s + K_y/K_{\dot{y}})(s + 1/T_{wo})}{s^3(s + 1/\tau)} = 0 \qquad (34)$$

A generic sketch of the locus of the roots of $N_{\delta_w}^{FD}$ as a function of the roll gain, K_φ, is given in Fig. 28. The "desirable locus" (solid lines) reflects the need for a low-frequency, well-damped, second order (ω_{FD}') to maximize the K/s region in the effective controlled element. Consideration of the factors required to obtain the desirable locus gives rise to the observations and system tradeoffs shown in Table 6. From Table 6 it is clear that the parameters $K_y/K_{\dot{y}}$, $1/T_{wo}$, and τ must be minimized only to the extent that a "desirable locus" is attained and in such a way that the system conflicts are acceptably resolved. To this extent several combinations of these parameters were picked and tested via the measures in Table 5.

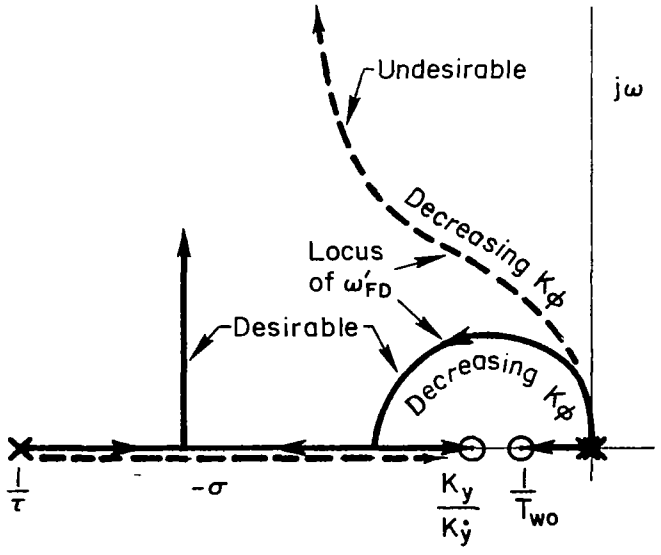

Figure 28. Generic Root Locus for Factoring $N_{\delta_w}^{\varphi}$ ($K_p = 0$)

TABLE 6. PARAMETER ADJUSTMENT TRADEOFFS

REQUIRED FOR "DESIRABLE LOCUS"	OTHER SYSTEM CONSIDERATIONS
Minimize $K_y/K_{\dot{y}}$	Very low values of $K_y/K_{\dot{y}}$ result in poor response quality due to "long tails" during capture. ($e^{-K_y/K_{\dot{y}}t}$ is the dominant mode at low frequency.
Maximize T_{wo}	Bank angle must wash out faster than the dominant path mode (ω_{FD}) to minimize residual feedback which will result in standoffs with y_ϵ.
Minimize τ	The break frequency of the beam rate filter is $1/\tau$, and as such, requires τ be kept large enough for adequate noise rejection.

The final parameter adjustment involved setting the roll rate feedback, K_p, to maximize the region of K/s in the effective controlled element. Again root locus factoring was used to gain an appreciation of the effect of varying K_p on the FD_w/δ_w numerator. A generic sketch of the root locus factoring of Eq. 33 with "optimum values" of $K_y/K_{\dot{y}}$, T_{wo}, and τ is given in Fig. 29.

This sketch indicates that increasing p feedback has a deleterious effect on the dominant path mode zero, i.e., tends to increase ω_{FD} and decrease ζ_{FD}. This effect may be explained as follows. Assuming the crosscoupling between r and p to be small ($\dot{\varphi} >> r \tan \theta_o$), the relationship between bank angle, φ, and the actual feedback quantity, φ_{wo} (see Fig. 27), is given by the approximate Bode asymptotes of G_φ (for $1/T_{wo} << K_\varphi/K_p$) in Fig. 30. These asymptotes indicate that pure bank angle feedback ($K_\varphi\varphi$) exists over a frequency region bounded by $1/T_{wo}$ and K_φ/K_p and that the feedback is essentially roll rate at all other frequencies. Thus, as K_p is increased, the effective feedback becomes the derivative of crosstrack acceleration, $\ddot{y}(\ddot{y} \doteq g\varphi)$, with the corresponding effect on the path mode shown in Fig. 29. While this effect exists on more conventional systems (FD A), it is more pronounced when the bank angle is washed out. As a result, it is necessary to strike a compromise between the pilot-centered requirement for K/s at high frequencies and path mode stability.

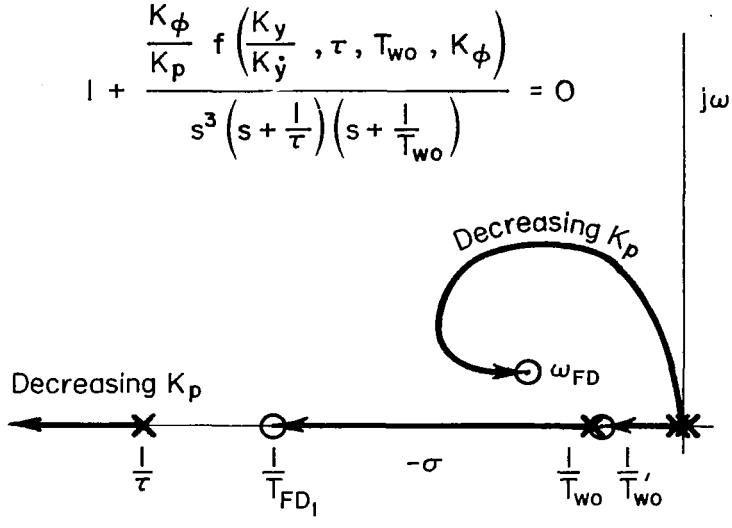

Figure 29. Generic Root Locus for Roots of $N_{\delta_w}^{FD} = f(K_p)$

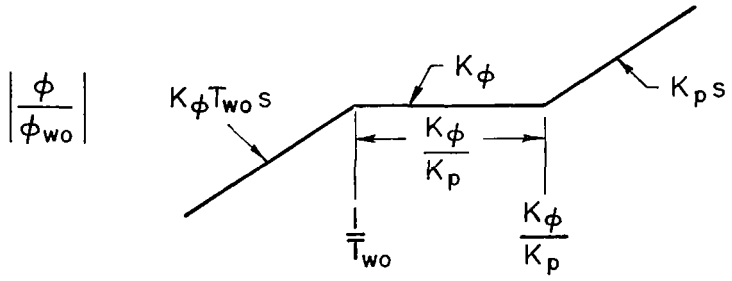

Figure 30. Approximate Bode Asymptotes of G_φ

With the above considerations in mind, the system parameters were adjusted to give the controlled element characteristics shown in Fig. 31. The crossover frequency shown was estimated from the FSAA simulator time responses. (Notice that it corresponds to near-maximum phase margin.)

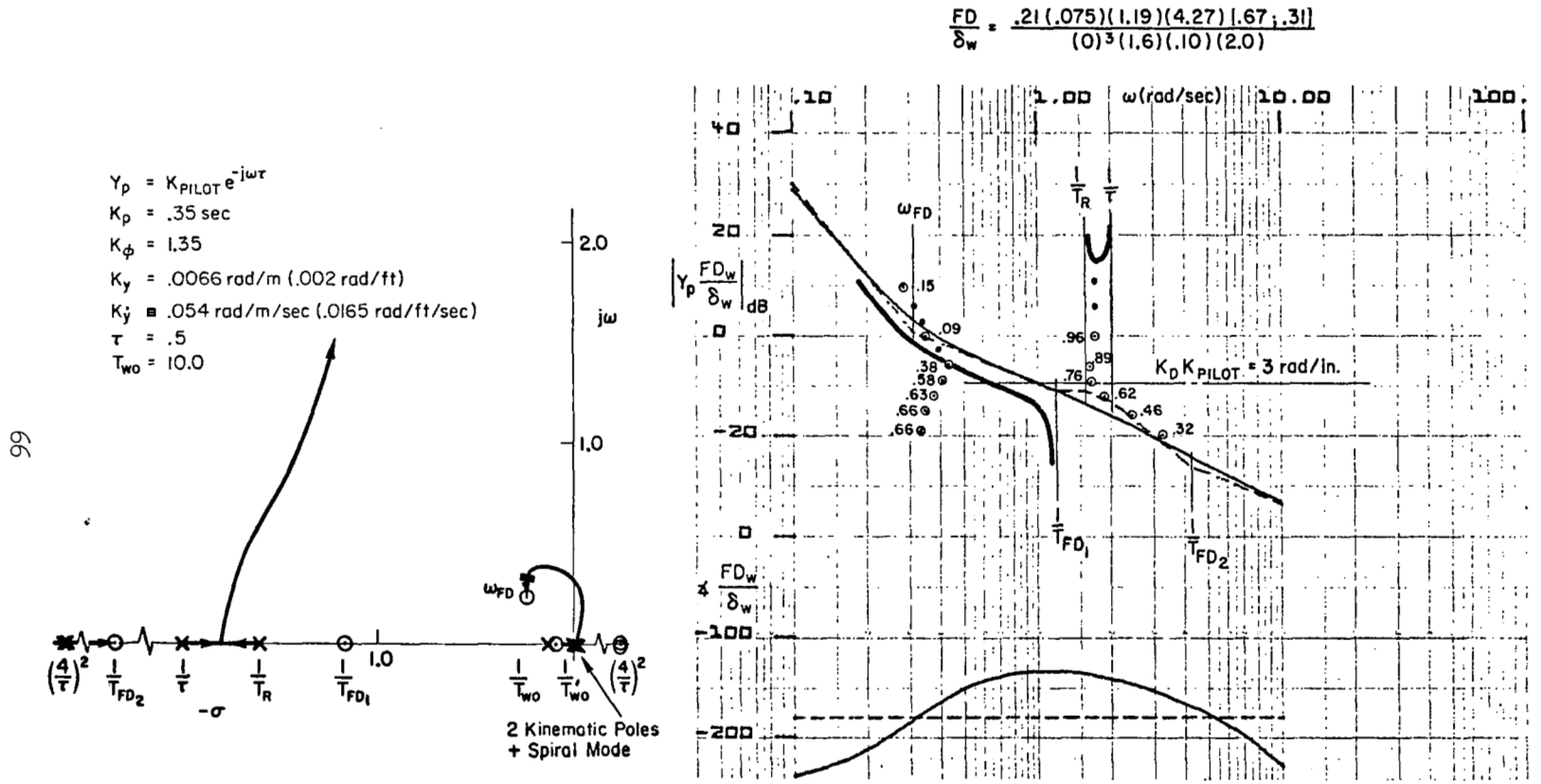

Figure 31. System Survey for Flight Director B, $Y_p(FD/\delta_w)$

The compromise involved in setting the p feedback gain is evident from the region of K/s^2 between $1/\tau$ and $1/T_{FD_2}$ in the Bode asymptotes.

Comparison of the Bode amplitudes between FD A and FD B indicates that FD B is down by a factor of 1.5 in the region of crossover. Piloted simulator experiments indicated that this was too low and the display gain was therefore set to 1.5.

As in FD A, the low-frequency conditional instability was found to have no effect on pilot opinion.

The initial condition response characteristics of FD B are given in terms of the time and frequency characteristics in Fig. 32. Focusing first on the closed-loop frequency response (Fig. 32a), the mid-frequency response is seen to be primarily second order at ω'_{FD}. The effect of the bank angle washout shows up as a low-frequency droop in the frequency response. We would therefore expect that all but a small part of any lateral offset will be eliminated at frequency ω_{FD} (0.41 rad/sec), and the remainder as a first-order decay with time constant $1/T_s$ (closed-loop spiral mode). This is borne out in Fig. 32b where it is seen that all but 5 percent of the lateral offset is removed in 12 seconds and that the last 5 percent 6.1 m (20 ft) seems to stand off, but in fact goes to zero in $3T_s = 43$ sec. This effect is inherent to the washed-out system and is attributable to the residual output of the washout circuit which causes an effective standoff with y_ϵ (compare φ and φ_{wo} in Fig. 32b). The low-frequency droop may be minimized by driving the spiral mode directly into the washout zero as in Fig. 28. Note that this implies $K_y/K_{\dot{y}}$ should be set equal to or greater than $1/T_{wo}$, which in effect sets an upper limit on $1/T_{wo}$. The residual lateral offset in Fig. 32b was found to be negligible during the simulator evaluations of FD B.

The disturbance regulation characteristics to crosswind shear for FD A and FD B, compared in Fig. 33, indicate that regulation against crosswind shear is considerably improved with FD B. However, this is compromised by a slightly degraded response when correcting for a lateral offset in the presence of a negative crosswind as shown in Fig. 34. From a practical standpoint, it is more likely that the aircraft will encounter a crosswind shear while tracking the localizer than correcting for large offsets in the

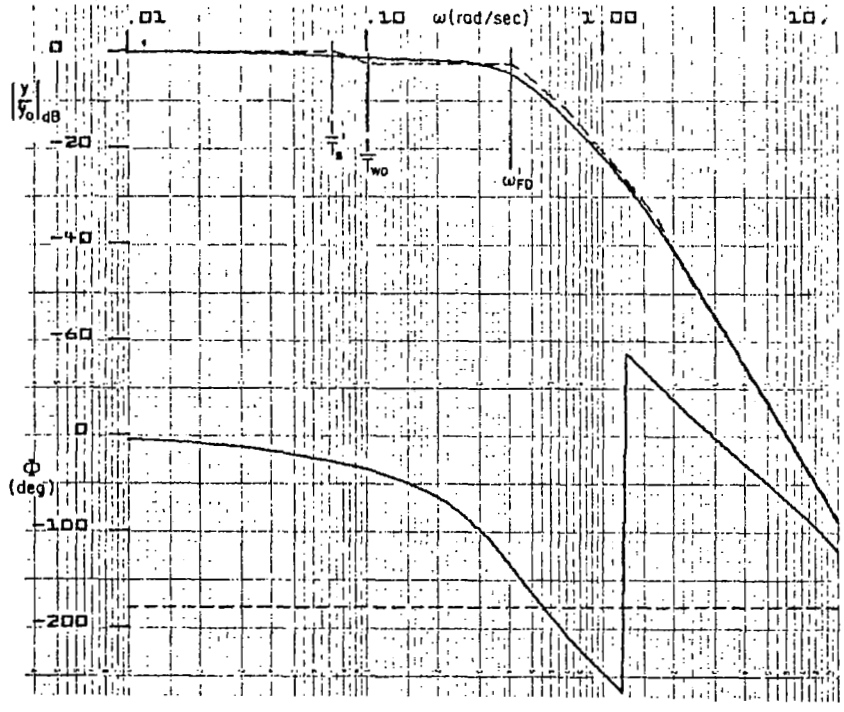

a) Closed-Loop Frequency Response of Crosstrack Error to an Initial Condition (FD B)

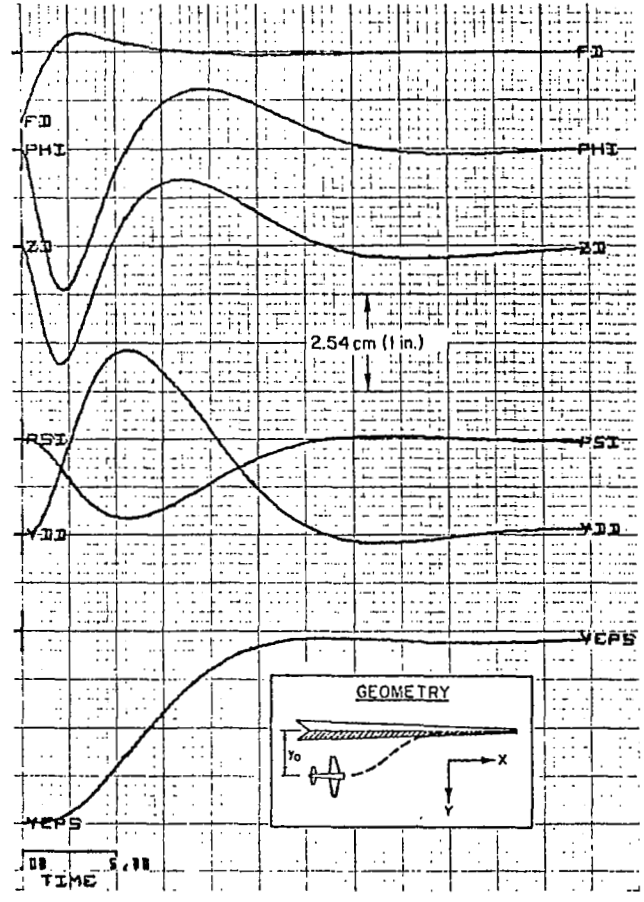

b) Initial Condition Response for FD B

Figure 32. FD B Characteristics

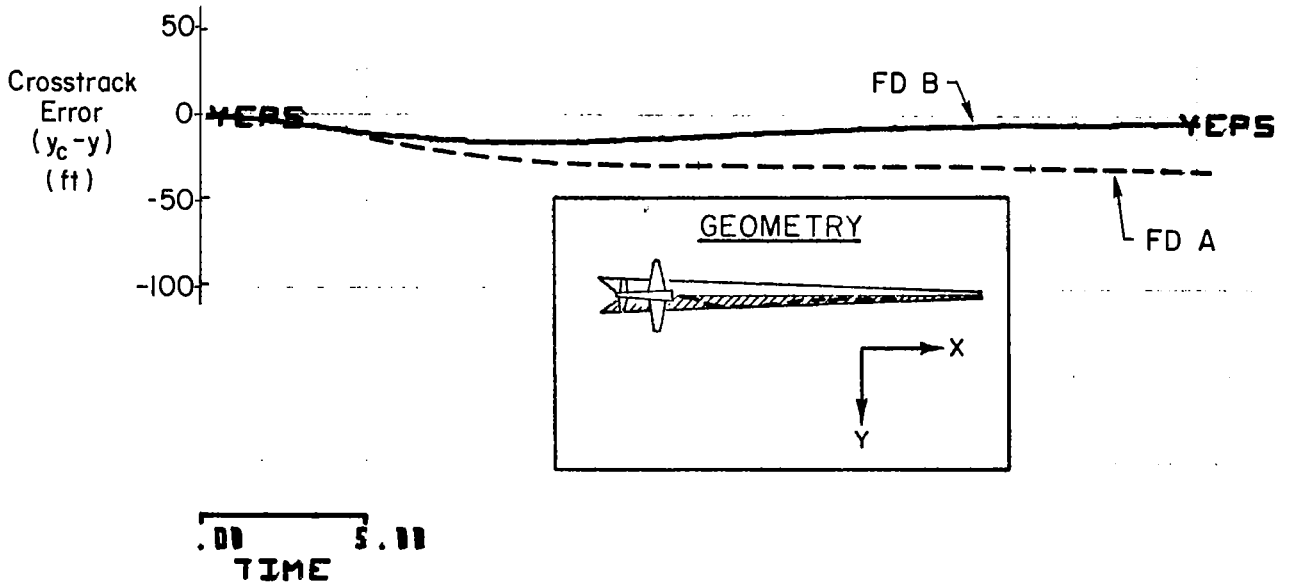

Figure 33. Comparison of FD A and FD B Response to a Crosswind Shear of .68 m/sec^2 (2.23 ft/sec^2)

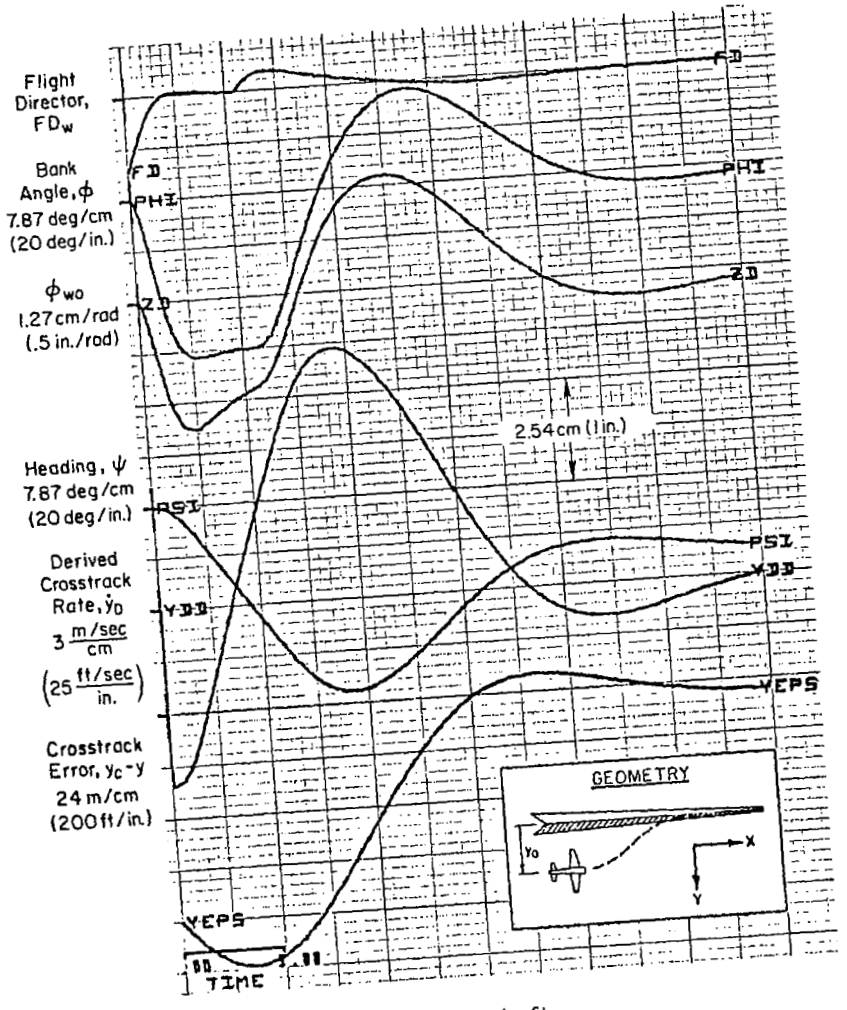

a) Crosswind From Left

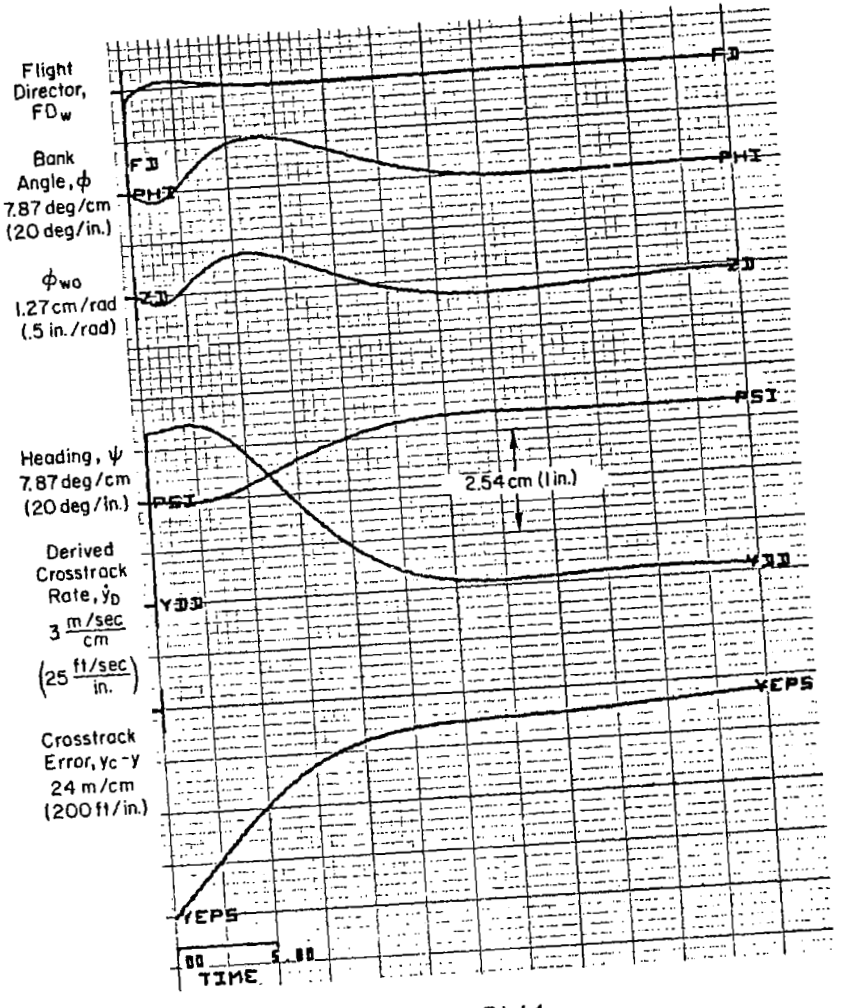

b) Crosswind From Right

Figure 34. FD B Response to an Initial Condition Offset with a 25 kt Crosswind

presence of a steady wind. This is especially true when the aircraft is near touchdown (or decision height). It is therefore felt that the slower response time in a right crosswind (compare Figs. 25b and 34b) is not a significant drawback when compared to the improved response to wind shear shown in Fig. 33.

The fundamental advantage of the washed-out bank angle director lies in its ability to track an arbitrary course (within design limits) without the benefit of external guidance inputs in the form of feedforward commands. The time response characteristics of a curved course intercept from a straight course are shown in Fig. 35 in calm air and with a 25 kt tailwind. These results are for a 1219 m (4000 ft) turn radius and a true airspeed of 90 kt. Course transients at the intercept point are inherent due to the lack of an advanced bank angle command and are sensitive to the commanded turn radius, true airspeed, and wind.

E. ERROR ANALYSIS FOR FD B

The dominant tracking errors are seen to occur at curved path intercept. These errors are induced by the fact that the required bank angle is not achieved until several seconds after the intercept point. This "effective time delay" is a function of the maximum roll rate and pilot reaction time. It is accounted for in the FD A design by initiating the bank angle command a small time increment before curved course intercept. Since the basic concept of FD B is to free the system from trajectory-dependent logic, this feedforward "lead" is not desirable. The following error analysis applies to any lateral flight director where bank angle is not commanded before curved course intercept.

If we simplify the bank angle response to a constant step of magnitude Φ, occurring ΔT sec after the curved course intercept, the path geometry may be represented as shown in Fig. 36.

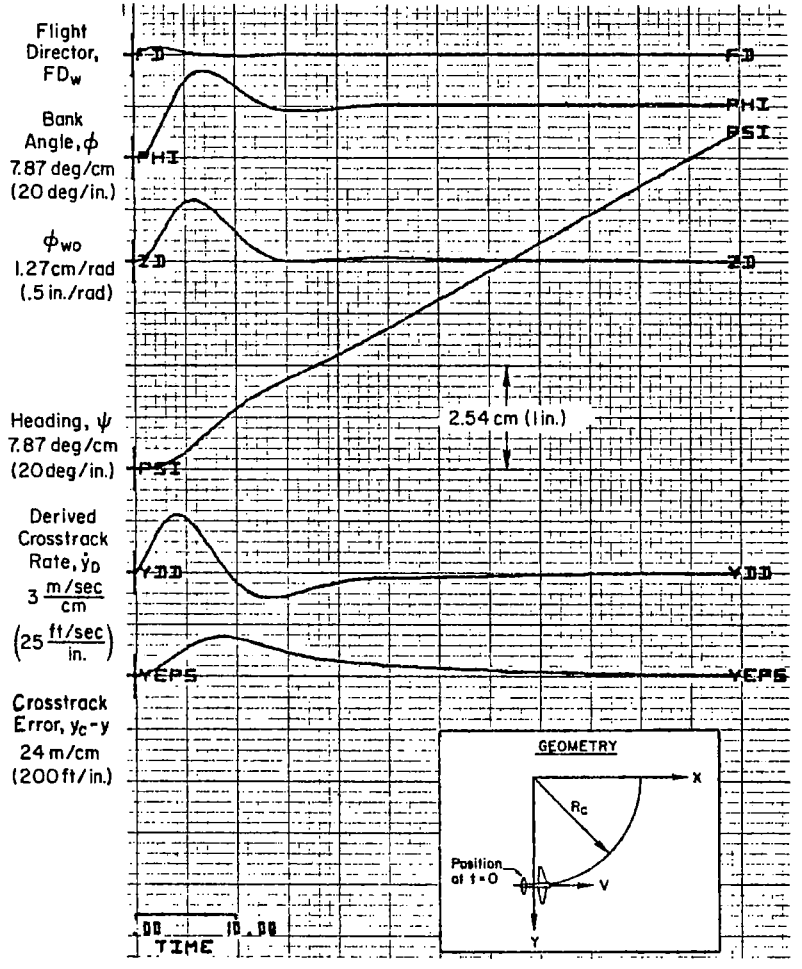

a) No Wind

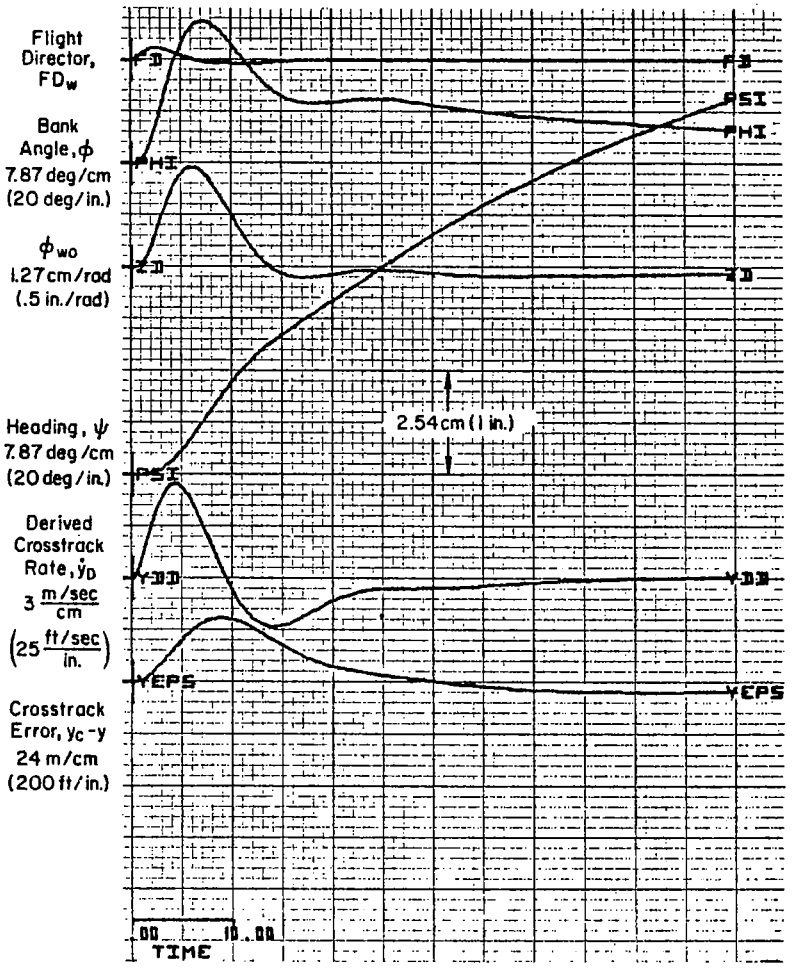

b) 25 kt Tailwind

Figure 35. Flight Director B Curved Course Intercept, R_c = 1219 m (4000 ft), V = 90 kt

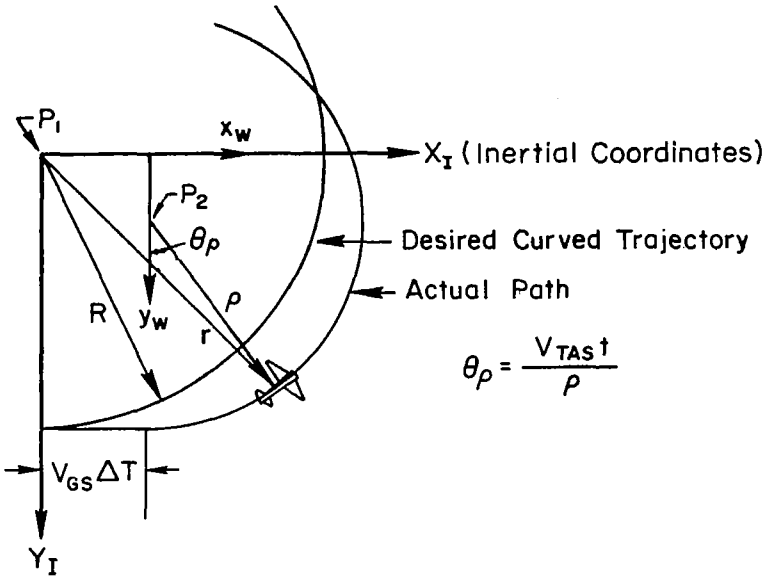

Figure 36. Geometry of Curved Path Intercept

The following definitions apply to Fig. 36:

P_1 = Center of the desired circular trajectory, fixed inertially

P_2 = Center of the osculating circle* which defines the actual path; moves with $x_w y_w$ frame

R = Radius of the commanded path

ρ = Inverse radius of curvature defined by the aircraft bank angle and speed as follows:

$$\rho \doteq V_{TAS}^2/\Phi g$$

r = Vector defining the aircraft position in the inertial frame

x_w, y_w = Coordinates fixed in the air mass

*An osculating circle is simply a circle defined by the radius of curvature at any point in an arbitrary curve (in this case the aircraft trajectory).

The maximum course overshoots occur with a tailwind at course intercept. In this case the $x_w y_w$ coordinate frame translates to the right at the wind speed, V_w, along the inertial x axis. The position of the aircraft in each of the coordinate systems is given as follows:

$$\begin{aligned} y_w &= \rho \sin \theta_\rho \\ x_w &= R - \rho(1 - \cos \theta_\rho) \\ X_I &= x_w \\ Y_I &= V_w t + \rho \sin \theta_\rho + V_{GS}\Delta T \\ \theta_\rho &= V_{TAS} t/\rho \end{aligned} \tag{35}$$

The crosstrack error is given as:

$$\begin{aligned} y &= r - R \\ &= (X_I^2 + Y_I^2)^{1/2} - R \end{aligned} \tag{36}$$

Since R is constant, the problem becomes one of finding the maximum value of r. Taking the derivative of r^2 and setting the resulting expression to zero results in an equation for t_{max}, the time when peak r occurs.

$$[V_{TAS}(R-\rho) - \rho V_w] \sin \frac{V_{TAS} t_{max}}{\rho} = (V_w t_{max} + V_{GS}\Delta T)\left(V_w + V_{TAS} \cos \frac{V_{TAS} t_{max}}{\rho}\right) \tag{37}$$

Values of t_{max} are solved from Eq. 37 using Newton Raphson iteration. The resulting t_{max} is used to compute y_{max}, the peak crosstrack error. Solutions for the peak crosstrack error were obtained by solving Eq. 37 for t_{max} and using the resulting values in Eq. 36. These results are shown in Fig. 37 for effective time delays of 3 and 6 sec, a true airspeed of 90 kt, and steady tailwinds of 0, 10, and 25 kt. Additionally, the aircraft was assumed to roll to the bank angle limit, i.e., Φ = 30 deg. The major conclusions to be drawn are:

1. The knee of the curves occur between 914 m (3000 ft) and 1219 m (4000 ft) turn radius. Therefore, commanded radii of less than 1219 m (4000 ft) are not deemed practical without an advanced bank angle command.

2. The sensitivity to tailwind magnitude increases rapidly as the commanded radius is decreased.

3. Peak crosstrack errors are quite sensitive to the time required to reach the required bank angle, i.e., to ΔT. (ΔT = 3 sec is consistent with measurements from piloted simulation.)

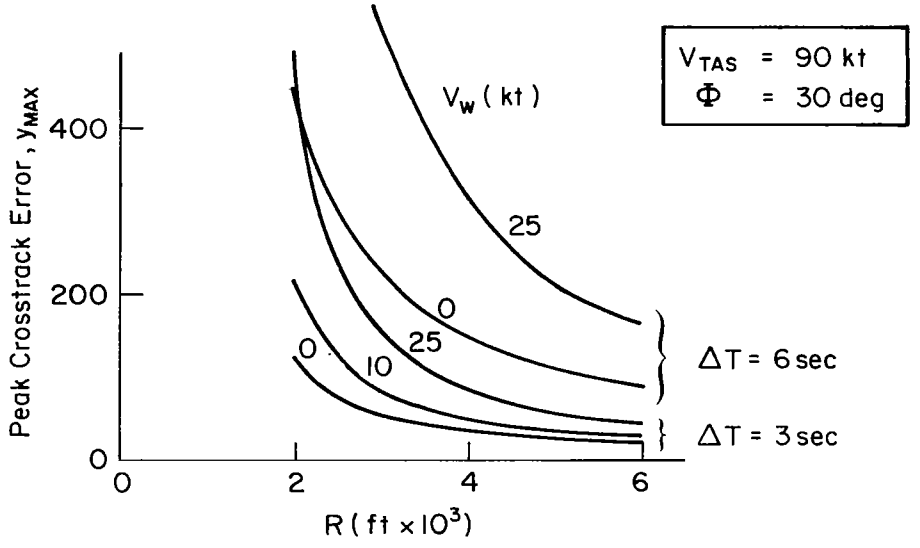

Figure 37. Peak Crosstrack Deviation

Note that when the peak crosstrack errors are small, the bank angle limit may not be reached (i.e., $\Phi \neq 30$ deg), resulting in a slightly larger error than predicted in Fig. 37.

As shown in the above analysis, the crosstrack errors become unacceptably large at curved course intercept when the commanded radius, R_c, is less than 1219-m (4000 ft). This problem may be alleviated in FD B by adding a constant washed-out step bank angle command to be initiated at the appropriate

time (approximately 3 sec) prior to course transition. As in FD A, the command signal magnitude is $\tan^{-1} V_{GS}^2/Rg$ and is passed through a second-order lag for smoothing (see Fig. 38). The simplification arises from the fact that the input is a constant and, because of the washout, is not

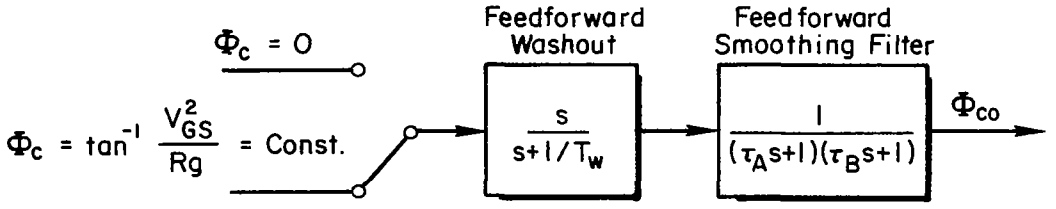

Figure 38. Simplified Feedforward for FD B

sensitive to errors in computed groundspeed. The feedforward in Fig. 38 is required only for turn radii less than 1219 m (4000 ft). Since the overall objective of FD B is to maintain design simplicity, and since turn radii of less than 1219 m (4000 ft) are unlikely in practice, the feedforward is not considered a basic part of the FD B design. It is given here as a possible "fix" in the event that small turn radii are required.

SECTION VI

SUMMARY AND CONCLUSIONS

A technique for the design of an integrated configuration management/ flight director system for powered-lift STOL's has been developed and proven using the NASA Ames Augmentor Wing as an example vehicle. A fundamental mission requirement was to allow manual tracking of a curved ILS beam including the capability for deceleration on the glide slope. In summary, the system which evolved from the resulting design-analysis effort consists of:

- A configuration management system involving a flap to hot thrust vector angle interconnect with both of these controls automatically driven by the airspeed sensor output.
- A longitudinal flight director consisting of a pitch command bar, and a throttle command bug.
- Two competing lateral flight director systems which allow tracking of curved paths.
- A rate command/attitude hold pitch SAS.

The resulting system was deemed very desirable by the pilots in that workload was reduced to an acceptable level and minimal compensation was required to obtain the desired performance.

Several important conclusions relating to the implications for future designs are summarized below.

- The concept of changing control techniques during the approach (frontside to backside) via the flight director was acceptable to the pilots.
- The pilot-centered requirement for "frequency separation of controls" was found to be extremely important for pilot acceptance. That is, if more than one control is commanded in a single axis, the secondary command must be at a low enough frequency so as to be considered a trim function by the pilot (e.g., well below the path mode frequency). In the present system the throttle director was secondary during frontside control ($V_{IAS} \geq 80$ kt) and the column director was secondary during backside tracking ($V_{IAS} \leq 79$ kt).

- A speed SAS (airspeed to hot thrust vector angle in the example system) was necessary to satisfy the frequency separation of controls requirement and still achieve acceptable airspeed control. Attempts to allocate the airspeed control function solely to the column director resulted in an unacceptably high level of activity for a secondary control (excessive pilot workload). A low gain airspeed feedback to the column director was acceptable in that it acted as an attitude trim function to help regulate against large disturbances which saturate the speed SAS.

- When operating in the backside mode, the configuration management system must not require discontinuities in trim power.

- The effective controlled element which consists of the SAS + airplane + primary flight director must have a K/s slope (in the frequency domain) in the region of piloted crossover. A pure gain shape was acceptable for the throttle director but was not as desirable as the K/s system.

- An angle-of-attack protection circuit (angle of attack to throttle command when angle of attack exceeds 10 deg for the example airplane) was required.

- Low deceleration capability on steep (−7.5 deg) approach paths is an inherent STOL limitation unless auxiliary drag devices are employed.

- The lateral flight director must command the bank angle 3 sec before curved course intercept for turn radii of less than about 1219 m (4000 ft).

- The HSI is not an adequate status display during curved path tracking. A moving map display is suggested as a solution to the display problem although this was not tested in the present program.

REFERENCES

1. Johnson, Walter A., Samuel J. Craig, and Irving L. Ashkenas, Analysis and Moving-Base Simulation of Transition Configuration Management Aspects of a Powered Lift STOL Aircraft, NASA CR-114698, Aug. 1973.

2. Klein, Richard H., Lee G. Hofmann, and Duane T. McRuer, Analytical Design and Simulation Evaluation of an Approach Flight Director System for the Augmentor Wing Jet STOL Research Aircraft, NASA CR-114697, Apr. 1973.

3. Weir, D. H., R. H. Klein, and D. T. McRuer, Principles for the Design of Advanced Flight Director Systems Based on the Theory of Manual Control Displays, NASA CR-1748, Mar. 1971.

4. Johnson, Walter A., and Samuel J. Craig, "Configuration Management During Transition for a Powered-Lift STOL Aircraft," J. Aircraft, Vol. 13, No. 2, Feb. 1976, pp. 119-122.

5. Klein, Richard H., and Warren F. Clement, Application of Manual Control Display Theory to the Development of Flight Director Systems for STOL Aircraft, AFFDL-TR-72-152, Jan. 1973.

6. McRuer, Duane, and David H. Weir, "Theory of Manual Vehicular Control," Ergonomics, Vol. 12, No. 4, July 1969, pp. 599-633.

7. McRuer, Duane T., and Ezra S. Krendel, Mathematical Models of Human Pilot Behavior, AGARD-AG-188, Jan. 1974.

8. McRuer, Duane, "The Development of Pilot-in-the-Loop Analysis," J. Aircraft, Vol. 10, No. 9, Sept. 1973, pp. 515-524.

9. Quigley, Hervey C., Robert C. Innis, and Seth Grossmith, A Flight Investigation of the STOL Characteristics of an Augmented Jet Flap STOL Aircraft, NASA TM X-62,334, May 1974.

10. McRuer, Duane, Irving Ashkenas, and Dunstan Graham, Aircraft Dynamics and Automatic Control, Princeton Univ. Press, 1973.

11. Hoh, Roger H., Richard H. Klein, and Walter A. Johnson, Design of a Flight Director/Configuration Management System for Piloted STOL Approaches, NASA CR-114688, Sept. 1973.

12. Hoh, Roger H., Samuel J. Craig, and Irving L. Ashkenas, Identification of Minimum Acceptable Characteristics for Manual STOL Flight Path Control. Vol. I: Summary Report, Systems Technology, Inc., Tech. Rept. 1035-3R-I, June 1976.

13. Clement, Warren F., Curved and Straight Course Equalization for Lateral Approach Control, Systems Technology, Inc., WP-1015-10, Oct. 1972.

14. Weir, David H., Compilation and Analysis of Flight Control System Command Inputs, AFFDL-TR-65-119, Jan. 1966.